

Plasma proteomics links brain and immune system aging with healthspan and longevity

Received: 31 May 2024

Accepted: 23 May 2025

Published online: 9 July 2025

 Check for updates

Hamilton Se-Hwee Oh^{1,2,3}✉, Yann Le Guen^{4,5}, Nimrod Rappoport⁶, Deniz Yagmur Urey^{2,3}, Amelia Farinas^{2,3,7}, Jarod Rutledge⁶, Divya Channappa^{2,3,4}, Anthony D. Wagner^{3,8}, Elizabeth Mormino⁴, Anne Brunet^{3,6,9}, Michael D. Greicius⁴ & Tony Wyss-Coray^{2,3,4}✉

Plasma proteins derived from specific organs can estimate organ age and mortality, but their sensitivity to environmental factors and their robustness in forecasting onset of organ diseases and mortality remain unclear. To address this gap, we estimate the biological age of 11 organs using plasma proteomics data (2,916 proteins) from 44,498 individuals in the UK Biobank. Organ age estimates were sensitive to lifestyle factors and medications and were associated with future onset (within 17 years' follow-up) of a range of diseases, including heart failure, chronic obstructive pulmonary disease, type 2 diabetes and Alzheimer's disease. Notably, having an especially aged brain posed a risk of Alzheimer's disease (hazard ratio (HR) = 3.1) that was similar to carrying one copy of *APOE4*, the strongest genetic risk factor for sporadic Alzheimer's disease, whereas a youthful brain (HR = 0.26) provided protection that was similar to carrying two copies of *APOE2*, independent of *APOE* genotype. Accrual of aged organs progressively increased mortality risk (2–4 aged organs, HR = 2.3; 5–7 aged organs, HR = 4.5; 8+ aged organs, HR = 8.3), whereas youthful brains and immune systems were uniquely associated with longevity (youthful brain, HR = 0.60 for mortality risk; youthful immune system, HR = 0.58; youthful both, HR = 0.44). Altogether, these findings support the use of plasma proteins for monitoring of organ health and point to the brain and immune systems as key targets for longevity interventions.

Aging causes organ dysfunction, chronic disease and death. Although interventions such as caloric restriction, young plasma and rapamycin extend healthspan in model organisms¹, potentially slowing aging, their human efficacy is unclear due to limited molecular understanding and assessment tools. Molecular biomarkers of human biological age linked to health and disease are needed.

Recent studies show that human organs age at different rates^{2–6}, as seen in animals^{7–9}, necessitating organ-specific biological age

measures. Prior estimates of organ age used clinical metrics and blood biochemistry, magnetic resonance imaging (MRI), DNA methylation or plasma proteins^{2–6}. However, their reproducibility across cohorts and over longitudinal visits, their sensitivity to organ-specific diseases and environmental factors and their associations with incident disease and mortality independent of each other and established aging biomarkers are unclear. Furthermore, it is unclear which organs are key to longevity in humans.

¹Graduate Program in Stem Cell and Regenerative Medicine, Stanford University, Stanford, CA, USA. ²The Phil and Penny Knight Initiative for Brain Resilience, Stanford University, Stanford, CA, USA. ³Wu Tsai Neurosciences Institute, Stanford University, Stanford, CA, USA. ⁴Department of Neurology and Neurological Sciences, Stanford University School of Medicine, Stanford, CA, USA. ⁵Quantitative Sciences Unit, Department of Medicine, Stanford University School of Medicine, Stanford, CA, USA. ⁶Department of Genetics, Stanford University, Stanford, CA, USA. ⁷Graduate Program in Neuroscience, Stanford University, Stanford, CA, USA. ⁸Department of Psychology, Stanford University, Stanford, CA, USA. ⁹Glenn Laboratories for the Biology of Aging, Stanford University, Stanford, CA, USA. ✉e-mail: hamilton.oh@mssm.edu; twc@stanford.edu

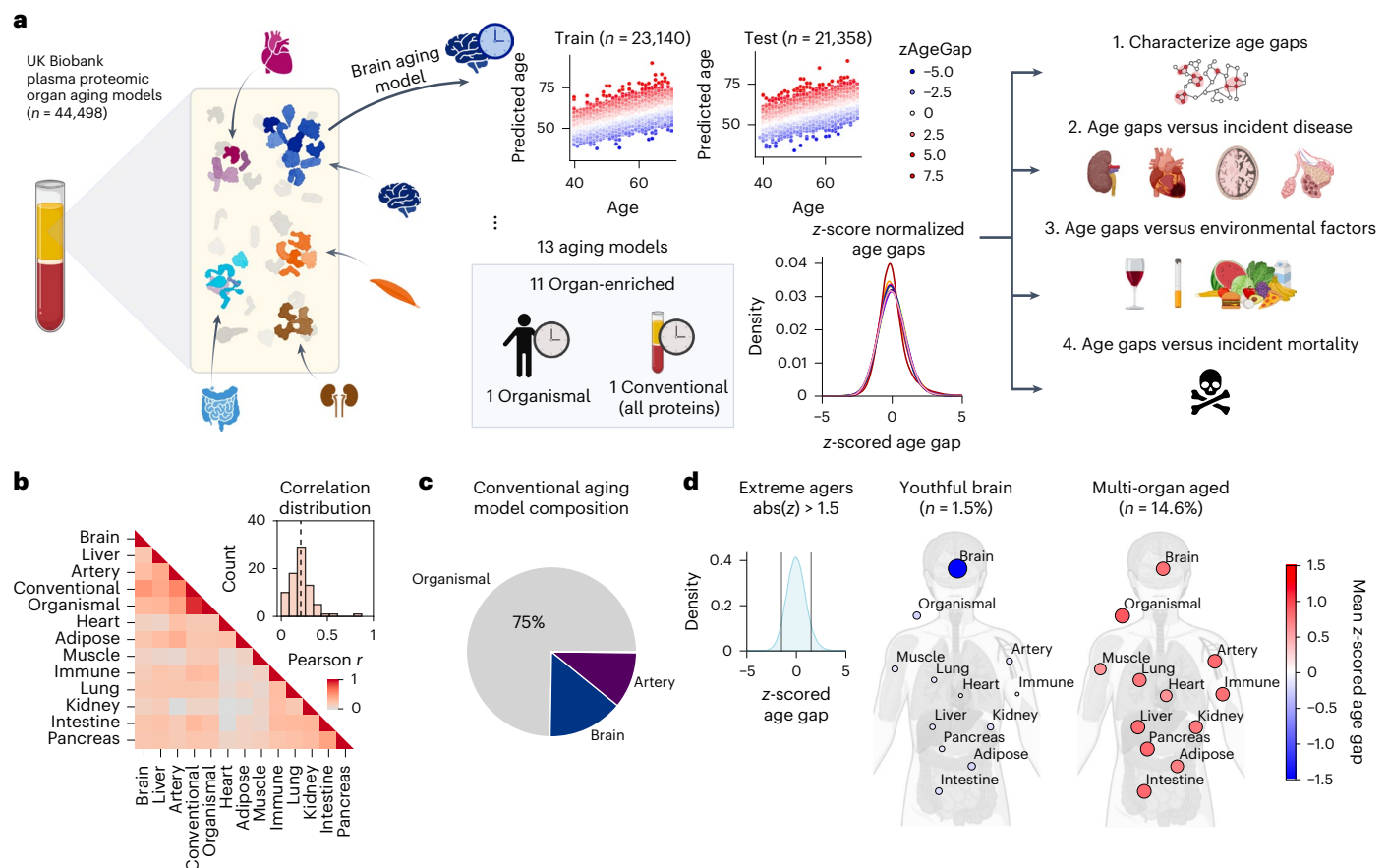


Fig. 1 | Plasma protein-derived organ age estimates in the UKB. **a**, Study design to estimate organ-specific biological age from plasma proteomics data in the UKB. A protein was called ‘organ-enriched’ if the gene encoding the protein was expressed at least four-fold higher in one organ compared to any other organ in the GTEx organ bulk RNA sequencing atlas. Organ-enriched protein sets were used to train LASSO chronological age predictors. Samples from 11 of 22 centers ($n = 23,140$) were used for training, and the remaining samples ($n = 21,358$) were used for testing. An ‘organismal’ model, which was trained on the levels of non-organ-specific (organ-shared) proteins, and a ‘conventional’ model, which was trained on all proteins from the Olink assay, were also developed and assessed. Model age gaps were calculated and then z-score normalized per organ to allow

for direct comparisons across organs. Age gaps were characterized and tested for associations with disease risk, modifiable lifestyle choices and mortality risk. **b**, Pairwise correlation of organ age gaps from all samples. Inset: the distribution of all pairwise correlations, with the dotted line representing the mean. **c**, A LASSO regression model was used to predict conventional age based on organ ages and organismal age. Organismal, brain and artery ages were sufficient to predict conventional age with $r^2 = 0.97$. Relative weights are shown as a pie chart. **d**, Extreme agers were defined by a 1.5-s.d. increase or decrease in at least one age gap. The mean organ age gaps of extremely youthful brain agers and accelerated multi-organ agers are shown. Graphics in **a** and **d** created with [BioRender.com](https://www.biorender.com).

Plasma proteomics, enabled by clinical accessibility of blood and advancing technologies, is ideal for gaining molecular insights into organ health and estimating organ-specific biological age. Building on our prior SomaScan-based study (5,678 individuals, 5,000 proteins)⁴, where we introduced machine learning models to estimate organ age, in the present study we tested our approach on 44,498 individuals in the UK Biobank (UKB) (age 40–70 years), using an orthogonal proteomics platform (Olink, ~3,000 proteins, 1,823 protein name overlap with SomaScan). These data were previously generated by the UKB Pharma Proteomics Project (UKB-PPP) and have been characterized in detail¹⁰.

The larger UKB cohort and expanded longitudinal phenotyping enabled us to explore organ age associations with a wider range of diseases (for example, chronic kidney disease, chronic obstructive pulmonary disease (COPD), heart failure and dementias) and focus on future disease incidence, which is a better proxy for biological age than disease prevalence. We also assessed sensitivity to environmental factors, including lifestyle, socioeconomic factors and medication use. Lastly, we performed a nuanced examination of mortality risk, comparing organ age estimates with established aging biomarkers, including PhenoAge and estimated glomerular filtration rate, and we

tested associations between extreme organ youth versus age acceleration on longevity versus early mortality.

Results

Plasma protein-derived organ age estimates in the UKB

To derive estimates of organ-specific biological age from the plasma proteome, we (1) identified plasma proteins likely derived from a specific organ (Supplementary Tables 1 and 2, Methods and Supplementary Fig. 1); (2) trained a machine learning model to predict chronological age based on the levels of identified organ-enriched proteins (Supplementary Tables 3 and 4 and Extended Data Fig. 1a); and (3) calculated the age gap based on each person’s predicted age (the relative predicted age compared to individuals of the same chronological age) (Methods and Fig. 1a). The age gap provides a measure of relative biological age compared to same-aged peers.

We performed these three steps for each of 11 major organs, including adipose tissue, artery, brain, heart, immune tissue, intestine, kidney, liver, lung, muscle and pancreas. We focused our analyses on these organs due to the availability of relevant age-related phenotype data in the UKB. To compare organ age gaps to organ-agnostic measures of biological age, we also derived age gaps from an ‘organismal’ aging

model trained on non-organ-specific proteins (80% of all proteins) and a 'conventional' aging model trained on all proteins on the Olink assay. We confirmed that the top proteins in the conventional aging model overlapped with a previous proteomic aging model developed on the UKB dataset¹¹.

Data from 11 of 22 plasma collection centers were used for model training and the remaining 11 for testing (Fig. 1a; see Methods and Supplementary Figs. 2 and 3 for details on protein quality control, imputation and modeling). Model performance was highly stable across train and test centers (Extended Data Fig. 2a,b and Supplementary Table 4). Age gaps were z-scored per aging model to allow for direct comparison between organs in downstream analyses (Fig. 1a). We observed some sex differences between organ age gaps, with males having older kidneys, immune systems and intestines and females having older adipose tissue, arteries and hearts (Extended Data Fig. 2c,d).

After deriving organ age gaps, we first determined the uniqueness of each measure. If organs age at different rates, then the age gap of one organ should be independent from the age gap of another. Pairwise correlations between age gaps showed that organ age gaps were only weakly correlated (mean $r = 0.21$; Fig. 1b and Supplementary Table 5), confirming previous studies^{3,4,6}. Organ age gaps differed from the conventional age gap, which strongly correlated with the organismal age gap ($r = 0.87$) due to majority protein overlap. Organismal, brain and artery ages explained 97% of conventional age variance, with organismal age contributing 74% (Fig. 1c).

We previously identified extreme organ agers who displayed especially fast aging in a single organ or in many organs⁴. We searched for extreme agers in the UKB by identifying individuals with age gaps above or below 1.5 s.d. from the population average in any organ (top and bottom -6–7% percentiles). Here we found not only fast (≥ 1.5 z-age gap) organ agers but also slow (≤ -1.5 z-age gap) organ agers (1–2% prevalence each, 33% total; Fig. 1d and Extended Data Fig. 2e). Differences between studies may stem from different sample sizes, proteomics platforms and thresholds. We also identified multi-organ agers who had two or more extreme organ age gaps (26% of samples; Extended Data Fig. 2e). Fourteen percent of samples were ambiguous, with both positive and negative extreme age gaps, and 27% of remaining samples were defined as normal agers (Extended Data Fig. 2e). Multi-organ agers were significantly older than normal and single-organ agers, suggesting that aged organs accumulate over time (Extended Data Fig. 2f).

To assess longitudinal stability of organ age gaps, we analyzed 1,176 individuals from the COVID-19 repeat imaging study with plasma proteomics (earlier version of Olink, 1,459 proteins) from 2–3 visits over 1–15 years (visits: baseline, Instance 2 and Instance 3) (Methods). Using organ aging models trained on the 1,459 proteins shared across Olink assay versions (correlated $r \geq 0.8$ with 3,000-protein models), we found moderate to strong correlations (mean $r = 0.6$) between baseline and Instance 2 visit age gaps, indicating relative stability over approximately 9 years, with potential dynamic changes due to lifestyle, disease or technical variability (Extended Data Fig. 3a).

Examining longitudinal stability of extreme ager status, we found that baseline extreme agers were 3–22 times more likely to remain extreme agers in the same organ at Instance 2 (Extended Data Fig. 3b), but 68% lost this status. Analyzing age gap changes in 0.5-s.d. bins, 76% of baseline extreme agers maintained directional stability at Instance 2 and 72% at Instance 3, supporting relative stability (Extended Data Fig. 3c–e). Additional studies with larger cohorts, denser sampling and higher-coverage proteomics are needed to clarify technical versus biological stability.

We next sought to compare our UKB Olink organ aging models with our previously developed SomaScan organ aging models. We generated Olink plasma proteomics data from 1,636 samples pooled across the Stanford Alzheimer's Disease Research Center (ADRC) and the Stanford Aging and Memory Study (SAMS)^{12,13}. We previously generated SomaScan plasma proteomics data from 601 of these samples for

our prior study⁴. This allowed us to directly compare organ age gaps derived across different proteomics platforms.

We tested UKB-trained organ aging models on Stanford Olink data. Of note, five organ aging model proteins—ANGPTL7, EBI3.IL27, GZMB, PGLYRP1 and ADIPOQ—had missing values in all Stanford samples (Extended Data Fig. 4a). EBI3.IL27 and ADIPOQ had relatively strong weights in the liver and adipose aging models, respectively (Extended Data Fig. 4a) and, therefore, reduced liver and adipose age prediction accuracy in the Stanford samples (Extended Data Fig. 4b). Overall, UKB-trained organ aging models showed similar age prediction accuracies across UKB-train, UKB-test and Stanford-test healthy control samples, demonstrating robustness of the models (Extended Data Fig. 4b).

We next compared organ age gaps between platforms. We observed moderate-strong correlations between the two platforms ($r = 0.3$ – 0.8 ; Extended Data Fig. 4c) with heart and kidney aging models displaying the most concordant age gaps across platforms ($r = 0.81$ and $r = 0.82$, respectively). The overall moderate correlations were expected given the differences in proteins measured per platform (1,823 proteins overlap, 1,093 Olink-specific, 3,156 SomaScan-specific) and the previously reported wide distribution of correlations for the overlapping proteins (by name) across the two platforms¹⁴ (Extended Data Fig. 4d). Even if the same protein by name is measured, the two platforms may quantify different forms of the same proteins (that is, isoform, posttranslational modification), which may not necessarily correlate with each other.

This suggested that each platform may provide complementary information in estimating organ age. Gene Ontology enrichment analyses showed that Olink brain aging proteins were enriched for perineuronal nets and glial differentiation, whereas SomaScan emphasized postsynaptic assembly; conversely, immune aging pathways were similar across platforms (Extended Data Fig. 4e). Both brain models were associated with prevalent Alzheimer's disease (Extended Data Fig. 4f), capturing distinct aging aspects. These findings show that organ-specific biological age estimates, likely related to organ health, can be derived from plasma proteomic data in the UKB.

Organ age estimates predict future age-related disease

For an estimate of biological age to be informative, it must robustly associate with the physiological state of the organ or individual and, consequently, with age-related health and disease outcomes. Hence, we sought to determine whether organ age gaps could predict future diseases in their respective organs. We tested the associations between all 13 z-scored age gaps and 15 incident age-related diseases (2–17-year follow-up) using Cox proportional hazard regression, while adjusting for age and sex. Following Benjamini–Hochberg correction for multiple hypothesis testing, we identified 176 positive and four negative significant associations out of 195 tests (Extended Data Fig. 5a and Supplementary Table 6).

We discovered highly significant associations between heart aging and atrial fibrillation (s.d. increase in heart age gap, hazard ratio (HR) = 1.75, $q < 1 \times 10^{-250}$) and heart failure (s.d. increase in heart age gap, HR = 1.83, $q = 8.35 \times 10^{-231}$), pancreas aging and kidney aging with chronic kidney disease (s.d. increase in pancreas age gap, HR = 1.80, $q = 3.36 \times 10^{-247}$; s.d. increase in kidney age gap HR = 1.66, $q = 2.85 \times 10^{-228}$), brain aging with Alzheimer's disease (s.d. increase in brain age gap, HR = 1.80, $q = 1.21 \times 10^{-67}$) and lung aging with COPD (s.d. increase in lung age gap, HR = 1.39, $q = 6.82 \times 10^{-49}$). Liver aging was associated with chronic liver disease (s.d. increase in liver age gap, HR = 1.20, $q = 3.87 \times 10^{-13}$), albeit the strength of the association was modest and similar compared to other organs. Notably, organ-specific age gaps consistently exhibited higher HRs than conventional age gaps across all diseases (Extended Data Fig. 5a).

The widespread significant associations between organ aging (176/195) and disease underscore the systemic nature of aging.

To disentangle these systemic effects and identify organ age associations with disease independent of aging in other organs, we examined multivariate Cox models that included all organ age gaps (excluding ‘conventional’ due to collinearity with ‘organismal’, $r = 0.87$) as covariates. After accounting for the aging of other organs, we found that organ age gap associations with disease became much more organ specific (Fig. 2a and Supplementary Table 7). For example, incident heart failure was associated with all 13 baseline age gaps individually but only seven age gaps independently. Counterintuitively, we observed that youthful arteries were associated with increased risk for many diseases, including type 2 diabetes (s.d. increase in artery age gap, HR = 0.68, $q = 2.11 \times 10^{-64}$), COPD (s.d. increase in artery age gap, HR = 0.85, $q = 8.85 \times 10^{-8}$), chronic liver disease (s.d. increase in artery age gap, HR = 0.87, $q = 7.58 \times 10^{-5}$) and others, highlighting the complexity of aging’s link with disease. Notably, Alzheimer’s disease was highly specific to brain aging, both individually (s.d. increase in brain age gap, HR = 1.80, $q = 1.21 \times 10^{-67}$) and independently of other organs (s.d. increase in brain age gap, HR = 1.91, $q = 2.37 \times 10^{-67}$).

We also investigated the associations between extreme organ ager status and disease risk, independent of age, sex and other extreme organs (Extended Data Fig. 5b and Supplementary Table 8). Multi-organ agers 5–7 and 8+ were not included due to limited sample size for most diseases. Individuals with 2–4 aged organs had significantly increased risk for every disease that we examined. Individuals with extremely aged brains, hearts, kidneys or lungs also showed broad increased risk of disease. Conversely, individuals with 2–4 extremely youthful organs were protected from many diseases, including chronic kidney disease, osteoarthritis and COPD. Among youthful organ profiles, the brain, immune system and intestine were nominally protective for at least four diseases (nominal $P < 0.10$). A youthful brain was especially protective of Alzheimer’s disease (extreme brain youth only, HR = 0.28, $P = 0.076$, $q = 0.24$) and other dementias, and a youthful intestine was especially protective of diabetes (extreme intestine youth only, HR = 0.30, $q = 3.63 \times 10^{-3}$; Extended Data Fig. 5b).

Given the brain’s strong and unique associations with Alzheimer’s disease, we further examined all individuals with extremely youthful or aged brains—regardless of single or multi-organ ager status—and their associations with Alzheimer’s disease risk, controlling for age, sex as well as *APOE* genotype, the strongest genetic risk factor of Alzheimer’s disease. Interestingly, we found that extreme brain aging conferred a 3.1-fold increase in Alzheimer’s disease risk (HR = 3.11, $P = 1.41 \times 10^{-28}$), and extreme brain youth conferred a 74% reduced risk of Alzheimer’s disease (HR = 0.26, $P = 4.37 \times 10^{-4}$), independent of age, sex, *APOE4* and *APOE2* (Fig. 2c,d). Consequently, individuals with aged brains exhibited a 13.5-fold increased risk of developing Alzheimer’s disease compared to those with youthful brains. Remarkably, when comparing the effects of brain age to *APOE* genotype, having an aged brain posed a risk similar to carrying one copy of *APOE4*, whereas having a youthful brain provided protection similar to carrying two copies of *APOE2* (Fig. 2c). Brain age was very weakly correlated with *APOE* genotype (Fig. 2e). Over the 17-year follow-up period, 120 of 2,628 individuals (4.56%) with aged brains developed Alzheimer’s disease, whereas only seven of 1,998 individuals (0.35%) with youthful brains developed the disease.

The specificity of the association between brain aging and dementia led us to investigate whether organ age gaps were associated with brain volume based on MRI data from follow-up visits (Extended Data Fig. 5c). We found that the brain age gap at baseline visit was uniquely associated with increased volume of the ventricles and decreased volume of cortical regions at Instance 2 (–9 years later on average).

Brain MRI data were previously used to derive estimates of biological brain age^{15,16}. To compare our plasma proteomic brain age estimate with an MRI-based brain age estimate, we trained an MRI brain aging model using 479 FreeSurfer brain volumetric phenotypes from 45,574 individuals from Instance 2. MRI brain age was correlated

with chronological age ($r = 0.81$, mean absolute error (MAE) = 3.65; Extended Data Fig. 5d), similar to previous reports^{15,16}. An s.d. increase in the MRI brain age gap conferred a 3.2-times increased risk of future Alzheimer’s disease (HR = 3.21, $P = 2.55 \times 10^{-36}$), confirming strong relevance to functional brain aging. Interestingly, however, MRI-based and plasma-based brain age gaps were only weakly correlated with each other ($r = 0.18$, $P = 2.50 \times 10^{-30}$; Fig. 2f), suggesting that each captures unique components of brain aging. Although this weak correlation is likely due, in part, to the approximately 9-year duration between MRI and plasma collection, a recent study showed that plasma brevican (BCAN) and glial fibrillary acidic protein (GFAP), but not other brain aging proteins identified in our study, were associated with MRI brain age¹⁷, suggesting that biological differences also contribute to the weak correlation. We speculate that MRI brain age captures global cell loss, whereas plasma brain age captures some of these volumetric changes as well as molecular alterations related to cell states and interactions.

We also assessed organ age gap associations with disease progression, by regressing age gaps against years since diagnosis, for individuals who were diagnosed with disease before blood draw. We found that many organ age gaps increased throughout chronic kidney disease progression (Extended Data Fig. 5e). Interestingly, the brain age gap was not associated with dementia progression (Extended Data Fig. 5f), suggesting that it captures age-related changes that may predispose individuals to dementia but does not reflect changes occurring after disease onset.

We next sought to gain further insights into organ aging by examining aging model proteins and their weights (Extended Data Fig. 1a). Aging models trained on the whole baseline sample versus only the randomly selected (86%) baseline samples resulted in essentially equivalent aging models and weights (Supplementary Fig. 4). The strongest weighted protein in the brain aging model was neurofilament light chain (NEFL; Fig. 2h), which increases with age and is a clinical biomarker of axon degeneration that is often measured in clinical trials for Alzheimer’s disease^{18,19} and was recently approved as a surrogate endpoint for a clinical trial to treat superoxide dismutase 1 amyotrophic lateral sclerosis (*SOD1* ALS)^{20,21}. Our data suggest that it, combined with other proteins, may also be a viable surrogate endpoint for brain aging and risk for dementia in normal people. Other highly weighted brain aging proteins include myelin oligodendrocyte protein (MOG), a component of the outer surface of myelin sheaths, and GFAP, a marker of reactive astrocytes, which both increased with age, as well as BCAN, a brain extracellular matrix component produced by oligodendrocyte precursor cells, and protein tyrosine phosphatase receptor type R (PTPRR), which both decreased with age (Fig. 2h). Plasma NEFL, GFAP and BCAN were previously highlighted as predictors of future dementia risk²². Using the permutation feature importance for biological aging (FIBA) algorithm⁴, we found that all of the top seven most highly weighted brain aging proteins contributed to the prediction of Alzheimer’s disease risk, showing the importance of leveraging the information from many brain-derived proteins to understand brain aging and disease risk (Extended Data Fig. 6a).

We then sought to determine which cell types these proteins were likely derived from by analyzing public human brain single-cell RNA sequencing data²³ (Extended Data Fig. 6b). Interestingly, we found that approximately half of brain aging proteins were specific to the oligodendrocyte lineage, with the rest expressed mostly in neurons and then astrocytes (Fig. 2i), pointing to white matter as a key aging region, as suggested by human brain MRI and mouse brain RNA sequencing studies^{24,25}.

Lung aging was explained primarily by lysosome-associated membrane glycoprotein 3 (LAMP3), a protein expressed specifically in type II alveolar stem cells; secretoglobin family 1A member 1 (SCGB1A1), also known as club cell secretory protein (CCSP), a marker of club cells; and C-C motif chemokine ligand 18 (CCL18), a cytokine expressed by alveolar macrophages, potentially reflective of stem cell dysfunction

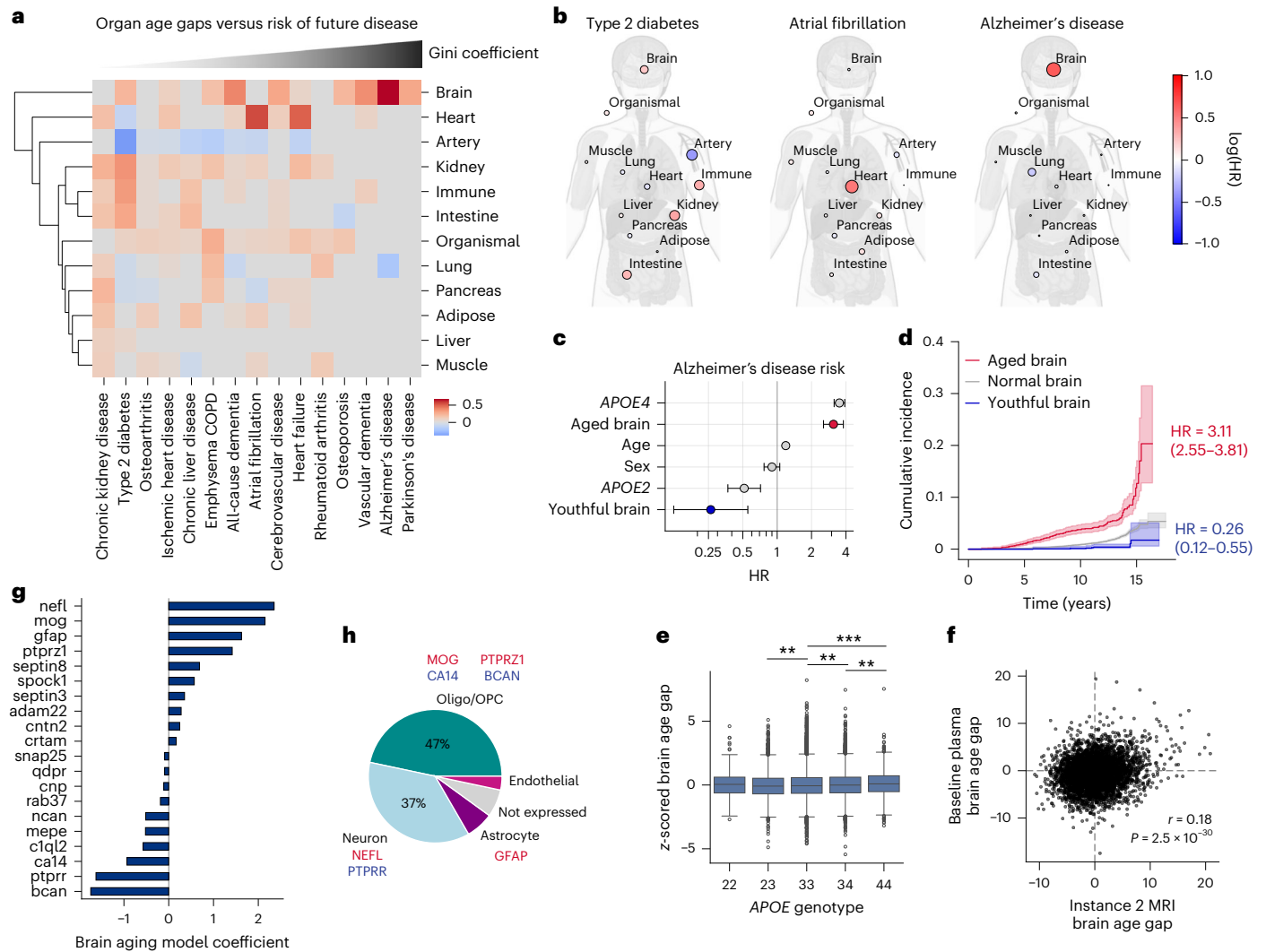


Fig. 2 | Organ age estimates predict future age-related disease. **a**, Cox proportional hazard regression was used to test the association between age gaps and future disease risk, adjusted for age-at-blood-draw, sex and other age gaps. The heatmap is color coded by age gap log(HR). Heatmap columns are ordered by the Gini coefficient of age gaps per disease. **b**, Body plots showing logHR values for type 2 diabetes, atrial fibrillation and Alzheimer's disease from the heatmap in **a**. **c**, Cox proportional hazard regression was used to test the association between extreme brain youth/aging and future Alzheimer's disease risk, adjusted for age-at-blood-draw, sex and *APOE4* and *APOE2* genotype ($n = 37,766$). Points show age gap HRs, and error bars show 95% confidence intervals. **d**, Cumulative incidence curves with 95% confidence intervals showing onset of Alzheimer's disease over time when comparing individuals with extremely aged brains, individuals with extremely youthful brains and normal brain agers. Age gap HRs and 95% confidence intervals from **c** are shown. **e**, Box plot visualization of brain age gap versus *APOE* genotype ($n = 43,326$). The box bounds are the Q1, median and Q3; the whiskers show Q1 – 1.5× the interquartile range (IQR) and Q3 + 1.5× the IQR. * $P < 0.05$, ** $P < 0.01$, *** $P < 0.001$ from standard two-sided *t*-test. **f**, Plasma-based brain age gap at baseline versus MRI-based brain age gap at Instance 2 (several years after baseline visit). Correlation and *P* value are shown. **g**, Bar plot displaying the top 20 protein coefficients in the brain aging model. **h**, Pie chart displaying the proportion of brain aging proteins assigned to each brain cell type based on single-cell RNA sequencing. Cell type was assigned based on cell type with the maximum expression of a given gene. Oligo, oligodendrocytes; OPC, oligodendrocyte precursor cell. Body graphic in **b** created with [BioRender.com](https://www.biorender.com).

and inflammation in the lung with age. Heart aging was explained primarily by N-terminal pro-B-type natriuretic peptide (NT-proBNP), a vasodilating hormone that increases in response to heart damage, whereas kidney aging was explained by renin (REN), a protein involved in blood pressure regulation. Both NT-proBNP and REN were previously identified as key heart and kidney aging proteins, respectively, based on SomaScan plasma proteomics data⁴ and are well-established biomarkers of heart and kidney function. All aging model protein weights are provided in Supplementary Table 3, and the top 20 proteins for each model are shown in Extended Data Fig. 1a. Together, these data show that plasma protein-derived organ age estimates are linked with age-related organ diseases and can reveal insights into the aging biology of their respective organs.

Organ age estimates are sensitive to modifiable lifestyle choices

We next explored whether biological age estimates grounded in physiological states of organ function are sensitive to changes in lifestyle. We tested the associations between all 13 z-scored age gaps and 18 lifestyle factors (that is, diet, alcohol, smoking, exercise and insomnia) and socioeconomic factors (that is, education and Townsend Deprivation Index), adjusted for each other as well as age and sex, using linear regression (Supplementary Table 9). We found 69 positive and 57 negative significant associations ($q < 0.05$) after correcting for multiple hypothesis testing. In line with their known health associations, smoking, alcohol, processed meat intake, the Townsend Deprivation Index and insomnia were associated with age acceleration across several organs,

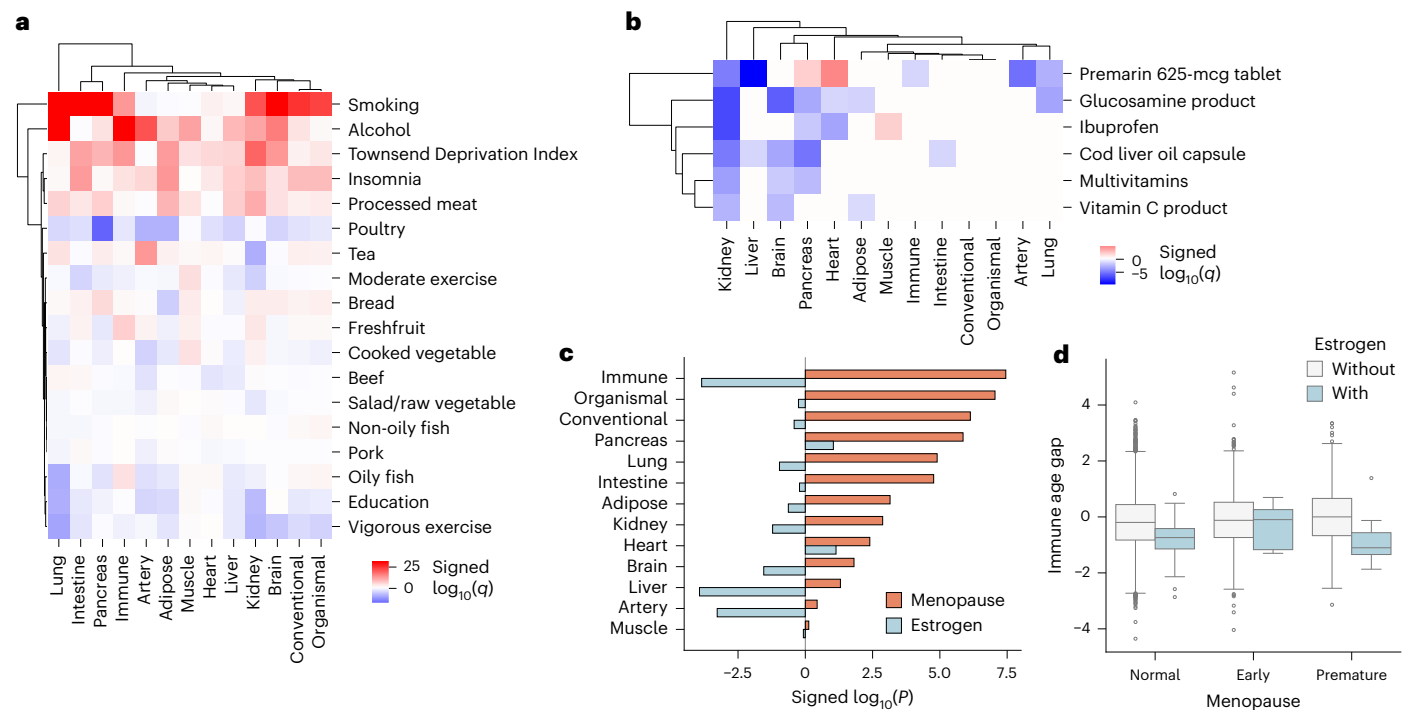


Fig. 3 | Organ age estimates are sensitive to modifiable lifestyle factors.

a, Linear regression was used to determine the association between age gaps and modifiable lifestyle factors while accounting for all other lifestyle factors as well as age and sex. The heatmap is color coded by signed $\log_{10}(q)$. Only significant ($q < 0.05$) values are indicated by color coding. **b**, Linear regression was used to determine the association between age gaps and drugs/supplements intake while accounting for age and sex. Only drugs with significant ($q < 0.05$) youthful associations in at least two organs are shown. Heatmap is color coded by signed

$\log_{10}(q)$ value. Only significant ($q < 0.05$) values are indicated by color coding. **c**, Multivariate linear regression was used to determine the association between age gaps versus early menopause and estrogen treatment independent of each other. Bar plot showing signed $\log_{10}(P)$ value for menopause and estrogen covariates is shown. **d**, Box plot visualization of immune age gaps in individuals stratified by menopause status and estrogen treatment ($n = 47$). The box bounds are the Q1, median and Q3; the whiskers show Q1 - 1.5 × the interquartile range (IQR) and Q3 + 1.5 × the IQR. Q, quartile.

whereas vigorous exercise, oily fish consumption, poultry consumption and higher education were associated with youthful organs (Fig. 3a).

We also tested the associations between all 13 z-scored age gaps and consumption of 137 drugs/supplements (n cases ≥ 100 ; Supplementary Table 10). After multiple hypothesis test correction, we found six products—Premarin, ibuprofen, glucosamine, cod liver oil, multivitamins and vitamin C—that were significantly ($q < 0.01$) associated with youth in at least two organs (Fig. 3b). Ibuprofen, glucosamine, cod liver oil, multivitamins and vitamin C products were associated with youth primarily in the kidneys, brain and pancreas (Fig. 3b).

Premarin is a conjugated estrogen medication typically prescribed to women experiencing postmenopausal symptoms, and estrogen medication was recently linked to reduced mortality risk in the UKB²⁶. Thus, we wondered whether estrogen medications may extend longevity by preventing menopause-induced accelerated aging of organs and disease risk²⁷. Among 47 women with normal, early or premature menopause treated with estrogen, earlier menopause was associated with accelerated aging across most organs (Fig. 3c), whereas estrogen treatment correlated with youthful immune, liver and artery profiles (Fig. 3d). Although cross-sectional analyses should be interpreted with caution, these findings underscore the sensitivity of plasma protein-derived organ age estimates to environmental factors and their potential for evaluating the effects of interventions.

Brain and immune system youth predict longevity

We next sought to determine whether organ age estimates were associated with future mortality. We tested associations between organ age gaps and all-cause mortality risk, adjusting for age and sex, over a 2–17-year follow-up using Cox proportional hazard regression (Supplementary Table 11). All organs showed significant associations,

with a 20–60% increased mortality risk per s.d. increase in age gaps (Fig. 4a), similar to findings from SomaScan-based organ aging models⁴. These associations were robust to adjustment with blood cystatin C, a marker of kidney filtration rate, and PhenoAge, an established blood biochemistry/cell-count-based biological age estimate (whose age gap has a mortality risk HR of 1.38 in the UKB), suggesting that organ age estimates provide independent information not captured by existing clinical biomarkers. Surprisingly, brain aging was most strongly predictive (s.d. increase in brain age gap, HR = 1.59, $P = 2.16 \times 10^{-293}$; Fig. 4a), suggesting that the brain may be a central regulator of lifespan in humans similar to findings in animal models (worms, flies and mice)^{28–30}. Indeed, individuals with aged brains had increased risk for several diseases beyond dementia, including COPD and heart failure (Extended Data Fig. 5a,b), consistent with previous studies showing that the brain regulates systemic inflammation^{31–35}.

To test whether organ age estimates provided additional predictive power, beyond cystatin C and PhenoAge, we compared concordance indices of mortality risk Cox models that included cystatin C, PhenoAge, organ ages or combinations, with age and sex as covariates. Organ ages alone performed similarly to the combined model, outperforming cystatin C and PhenoAge, indicating that they capture additional predictive information (Fig. 4b). Brain age, conventional age, PhenoAge and sex were key predictors in the combined model (Fig. 4c). Application of FIBA to understand contributions of brain and conventional aging model proteins on mortality risk highlighted BCAN, NEFL and PTPRR from the brain as well as ectodysplasin A2 receptor (EDA2R, organismal protein), chemokine C-X-C motif ligand 17 (CXCL17, organismal protein) and elastin (ELN, artery protein) from the conventional aging model as important proteins (Extended Data Fig. 6c–f).

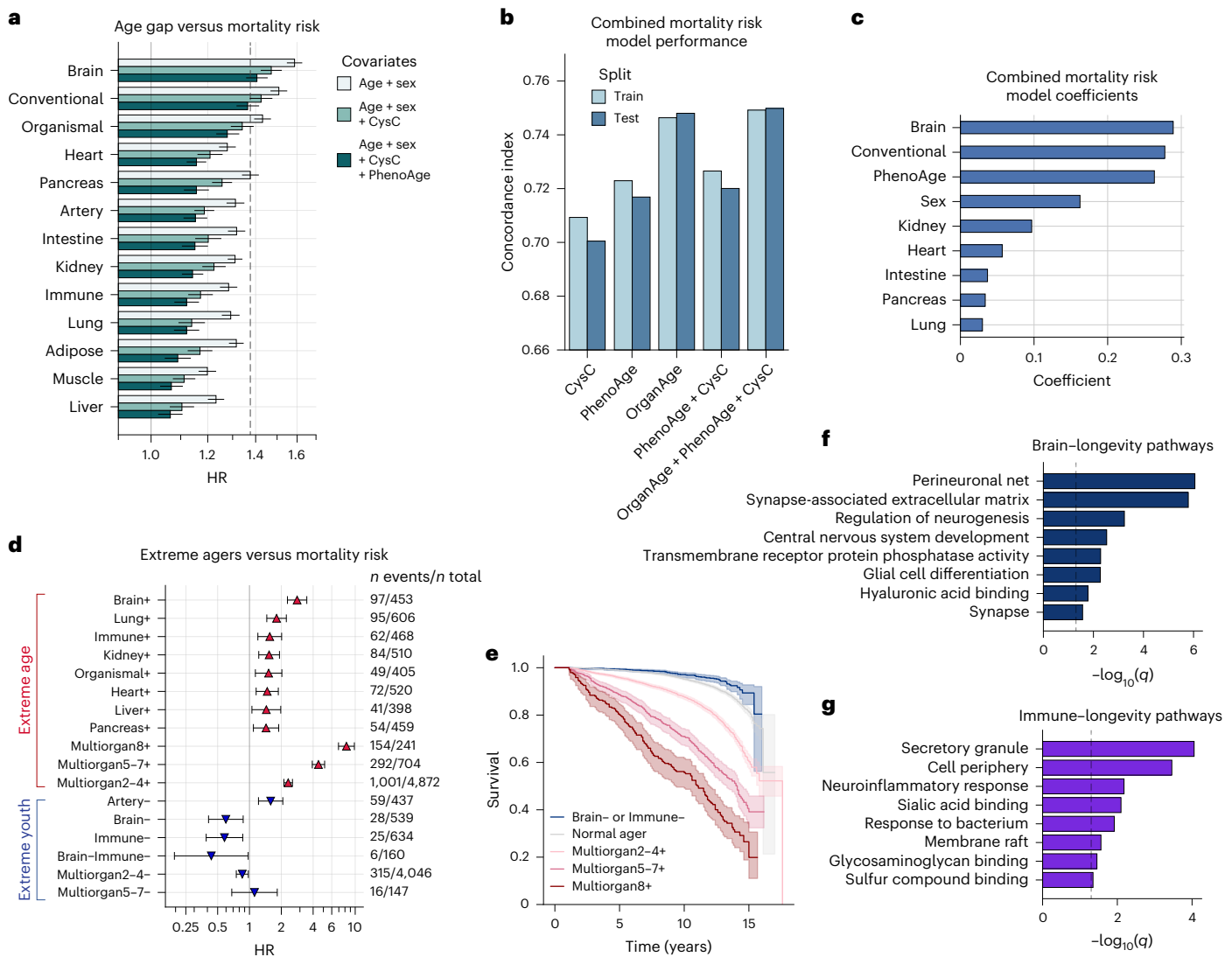


Fig. 4 | Accrual of aged organs progressively increases mortality risk, whereas brain and immune system youth is associated with longevity. **a**, Bar plot showing results from Cox proportional hazard regression analyses, testing the associations between each age gap and future all-cause mortality risk, controlling for labeled covariates ($n = 21,775$). Bars show HRs, and error bars show 95% confidence intervals. PhenoAge age gap HR adjusted for age and sex (HR = 1.38) is shown as a dashed line for reference. **b**, Concordance indices from various LASSO-regularized Cox proportional hazard models were trained to predict mortality risk. Performance across train and test centers is shown. Covariates for each model, in addition to age-at-blood-draw and sex, are labeled on the x axis. **c**, Model coefficients are shown for the combined model (OrganAge + PhenoAge + CysC) from **b**. **d**, Forest plot showing results from Cox proportional hazard

regression, testing the associations between extreme ager status ('+' refers to aged; '-' refers to youthful) and future all-cause mortality risk, controlling for age-at-blood-draw and sex. Only significant ($P < 0.05$) associations are shown. Points show extreme ager HRs; error bars show 95% confidence intervals; and the number on the right shows the number of events out of the total sample size. **e**, Kaplan-Meier curves with 95% confidence intervals showing survival over a 17-year follow-up for normal agers, multi-organ agers (with 2-4, 5-7 or 8+ aged organs) and individuals with a youthful brain or immune system (brain- or immune-). **f, g**, Gene Ontology pathway enrichment analyses from the top 10 brain (**f**) and immune (**g**) aging proteins, as determined from the mortality risk FIBA score (Methods). CysC, cystatin C.

Although each organ age gap was associated with risk of death, we wondered whether the accrual of aged organs would be increasingly detrimental. Hence, we tested whether single-organ extreme agers and multi-organ agers (bins of 2-4, 5-7 and 8+ organs) had an increased risk of death compared to normal agers, while adjusting for age and sex (Supplementary Table 12). Interestingly, we found that, whereas having a single aged organ (brain, lung, intestine, heart, immune, kidney, liver or pancreas) conferred a 1.5-3-fold increased risk of death, having 2-4, 5-7 and 8+ extremely aged organs conferred a 2.3-fold, 4.5-fold and 8.3-fold ($P = 2.05 \times 10^{-70}$, $P = 3.86 \times 10^{-106}$ and $P = 8.30 \times 10^{-127}$) increased risk of death, respectively (Fig. 4d,e). Notably, over 60% of individuals with 8+ extremely aged organs at blood draw died within 15 years (Fig. 4d).

We then sought to determine whether youthful organ profiles were associated with longevity (Supplementary Table 12). We found that individuals with youthful-appearing arteries had increased mortality risk, and those with multi-organ youth had no difference in mortality risk compared to normal agers (Fig. 4d). Using FIBA, we found that artery protein thrombospondin 2 (THBS2), a protein that decreases with age but has a positive association with mortality risk, was responsible for the nonlinear association between the artery age gap and mortality risk (Extended Data Fig. 6e). Why individuals with broad multi-organ youth are not protected is unclear, although this may be due to limited sample size.

Notably, though, individuals with youthful brains (HR = 0.60, $P = 7.49 \times 10^{-3}$) and immune systems (HR = 0.58, $P = 7.34 \times 10^{-3}$) had

significantly reduced mortality risk (Fig. 4d), similar to their unique protective associations with disease (Extended Data Fig. 5b). We, therefore, assessed individuals with both youthful brains and immune systems and found that this group was most strongly protected from mortality by effect size (HR = 0.44, $P = 0.042$; Fig. 4d,e), underscoring the benefits of having a resilient brain and immune system. Over 17 years, 792 of 10,000 (7.92%) normal agers died, whereas only six of 160 individuals (3.8%) with youthful brains and immune systems died.

To probe the underlying mechanisms implicated in brain-related and immune-system-related longevity, we performed Gene Ontology enrichment analyses of the top 10 brain and immune aging model proteins based on mortality risk FIBA scores (Fig. 4f,g and Extended Data Fig. 6h,i). Selection of brain-specific or immune-system-specific plasma proteins as background for the enrichment test did not result in significant associations, so we used all genes as background. Perineuronal net was the most enriched brain pathway (BCAN, PTPRZ1 and NCAN), and secretory granule was the most enriched immune system pathway. Intriguingly, neuroinflammation was another enriched immune system pathway, composed of metalloproteinase 9 (MMP9), a regulator of perineuronal net composition, as well as tumor necrosis factor receptor superfamily member 1B (TNFSRF1B) and integrin alpha M (ITGAM), also known as CD11B. Youthful brain agers had higher levels of BCAN and NCAN, and youthful immune agers had lower levels of MMP9 (Extended Data Fig. 6h,i), suggesting that global preservation of brain extracellular matrix partly due to reduced degradation by peripheral inflammatory factors and reduced chronic inflammation partly regulated by the brain could be crucial for promoting longevity. Together, these data reveal that plasma protein-derived organ age estimates improve upon existing aging biomarkers for mortality risk prediction, the accrual of aged organs progressively increases mortality risk, and a youthful brain and immune system are key to longevity.

Discussion

Our findings based on plasma proteomics data (~3,000 proteins) from nearly 45,000 individuals in the UKB establish plasma protein-derived organ age estimates as robust indicators of organ age, health and disease/mortality risk beyond gold standard clinical aging biomarkers and reveal key proteins implicated in the aging process. Furthermore, we show that organ age estimates are stable across train/test centers and longitudinal visits and are cross-sectionally associated with modifiable lifestyle choice, socioeconomic status and medications and, thus, lay the foundation for human experiments testing the effects of novel longevity interventions on the biological age of organs at the individual level.

We note key considerations and limitations to inform future work. Although our organ enrichment classification based on bulk RNA sequencing atlases yielded robust results, confirming the true protein sources remains challenging; high-resolution gene expression maps including information on alternative splicing and changes with age and disease could strengthen confidence. Like many studies, we relied on cross-sectional age gaps, which only approximate aging rate histories. Longitudinal proteomics data, integrated with deep environmental and genetic phenotyping, are essential to accurately measure aging rates, distinguish baseline differences and uncover their causes^{16,36–38}. Such data could also clarify the sequence of organ aging at individual and population levels. Although we observed that multi-organ aging increases with age, suggesting cumulative organ decline, the specific order of organ aging remains undefined. Surprisingly, individuals with highly youthful organ profiles (except for brain and immune system) were not protected from mortality, despite assumptions of benefit. This aligns with studies showing U-shaped associations between clinical biomarkers (for example, body mass index and platelet count) and mortality, where extremely youthful phenotypes are associated with elevated risk^{39–41}, warranting further exploration in aging biomarker research. Although organ age estimates independently predict mortality beyond clinical biochemistry biomarkers, their added

clinical value over established disease-specific biomarkers requires disease-by-disease investigation⁴². Finally, as UKB participants are predominantly of European ancestry, organ age estimates may need recalibration for diverse genetic and environmental contexts, necessitating broader studies.

In the present study, we found evidence that the brain and immune system may be central regulators of aging and longevity in humans, as aged brains are most strongly predictive of earlier mortality, and youthful brains and immune systems are uniquely predictive of longevity. After all, the brain regulates numerous critical age-related functions throughout the body, including circadian rhythm, blood pressure, energy homeostasis and stress response, via the neuroendocrine and autonomic nervous systems, and chronic inflammation has been heavily implicated in aging^{1,43}. Intriguingly, recent studies show bidirectional communication between the brain and immune system in aging and disease-relevant contexts, such as chronic stress, atherosclerosis and infection^{31–35,44}. These observations suggest that accelerated aging or maintenance of youth in the brain and immune system likely has broad age-related effects across the body, although additional studies are needed to test this hypothesis more rigorously in humans.

Regarding the molecular alterations that occur with brain aging, we found many unexpected age-associated and disease-associated changes in oligodendrocyte lineage and extracellular matrix proteins, implying extensive changes beyond neuroinflammation and neurodegeneration. Indeed, myelin degeneration and defective remyelination with mouse aging causes cognitive deficits⁴⁵ and aggravates Alzheimer's disease pathology⁴⁶, and microglia homeostatically modulate the perisynaptic matrix^{47,48}. Moreover, the observation that white matter regions exhibit the most pronounced shifts in aging microglial transcriptomes²⁵, coupled with the enrichment of genetic risk variants for neurodegenerative diseases in microglial and oligodendrocyte genes⁴⁹, underscores a potential link between oligodendrocyte aging and age-related neuroinflammation and their relevance to neurodegeneration. Future studies exploring these multicellular and extracellular matrix interactions in the aging brain and their interactions with the periphery may reveal key insights into human health and longevity.

Online content

Any methods, additional references, Nature Portfolio reporting summaries, source data, extended data, supplementary information, acknowledgements, peer review information; details of author contributions and competing interests; and statements of data and code availability are available at <https://doi.org/10.1038/s41591-025-03798-1>.

References

1. López-Otín, C., Blasco, M. A., Partridge, L., Serrano, M. & Kroemer, G. Hallmarks of aging: an expanding universe. *Cell* **186**, 243–278 (2023).
2. Ahadi, S. et al. Personal aging markers and ageotypes revealed by deep longitudinal profiling. *Nat. Med.* **26**, 83–90 (2020).
3. Tian, Y. E. et al. Heterogeneous aging across multiple organ systems and prediction of chronic disease and mortality. *Nat. Med.* **29**, 1221–1231 (2023).
4. Oh, H. S.-H. et al. Organ aging signatures in the plasma proteome track health and disease. *Nature* **624**, 164–172 (2023).
5. Sehgal, R. et al. Systems Age: a single blood methylation test to quantify aging heterogeneity across 11 physiological systems. Preprint at *bioRxiv* <https://doi.org/10.1101/2023.07.13.548904> (2023).
6. Goeminne, L. J. E. et al. Plasma protein-based organ-specific aging and mortality models unveil diseases as accelerated aging of organismal systems. *Cell Metab.* **37**, 205–222 (2025).
7. Herndon, L. A. et al. Stochastic and genetic factors influence tissue-specific decline in ageing *C. elegans*. *Nature* **419**, 808–814 (2002).

8. Schaum, N. et al. Ageing hallmarks exhibit organ-specific temporal signatures. *Nature* **583**, 596–602 (2020).
9. Rando, T. A. & Wyss-Coray, T. Asynchronous, contagious and digital aging. *Nat. Aging* **1**, 29–35 (2021).
10. Sun, B. B. et al. Plasma proteomic associations with genetics and health in the UK Biobank. *Nature* **622**, 329–338 (2023).
11. Kuo, C.-L. et al. Proteomic aging clock (PAC) predicts age-related outcomes in middle-aged and older adults. *Nat. Med.* <https://doi.org/10.1038/s41591-024-03164-7> (2024).
12. Trelle, A. N. et al. Hippocampal and cortical mechanisms at retrieval explain variability in episodic remembering in older adults. *eLife* **9**, e55335 (2020).
13. Trelle, A. N. et al. Association of CSF biomarkers with hippocampal-dependent memory in preclinical Alzheimer disease. *Neurology* **96**, e1470 (2021).
14. Eldjarn, G. H. et al. Large-scale plasma proteomics comparisons through genetics and disease associations. *Nature* **622**, 348–358 (2023).
15. Cole, J. H. Multimodality neuroimaging brain-age in UK biobank: relationship to biomedical, lifestyle, and cognitive factors. *Neurobiol. Aging* **92**, 34–42 (2020).
16. Leonardsen, E. H. et al. Genetic architecture of brain age and its causal relations with brain and mental disorders. *Mol. Psychiatry* **28**, 3111–3120 (2023).
17. Liu, W.-S. et al. Plasma proteomics identify biomarkers and undulating changes of brain aging. *Nat. Aging* **5**, 99–112 (2024).
18. van Dyck, C. H. et al. Lecanemab in early Alzheimer's disease. *N. Engl. J. Med.* **388**, 9–21 (2023).
19. Pontecorvo, M. J. et al. Association of donanemab treatment with exploratory plasma biomarkers in early symptomatic Alzheimer disease: a secondary analysis of the TRAILBLAZER-ALZ randomized clinical trial. *JAMA Neurol.* **79**, 1250–1259 (2022).
20. Miller, T. M. et al. Trial of antisense oligonucleotide tofersen for SOD1 ALS. *N. Engl. J. Med.* **387**, 1099–1110 (2022).
21. Irwin, K. E., Sheth, U., Wong, P. C. & Gendron, T. F. Fluid biomarkers for amyotrophic lateral sclerosis: a review. *Mol. Neurodegener.* **19**, 9 (2024).
22. Guo, Y. et al. Plasma proteomic profiles predict future dementia in healthy adults. *Nat. Aging* **4**, 247–260 (2024).
23. Haney, M. S. et al. APOE4 is linked to damaging lipid droplets in Alzheimer's disease microglia. *Nature* **628**, 154–161 (2024).
24. Fujita, S. et al. Characterization of brain volume changes in aging individuals with normal cognition using serial magnetic resonance imaging. *JAMA Netw. Open* **6**, e2318153 (2023).
25. Hahn, O. et al. Atlas of the aging mouse brain reveals white matter as vulnerable foci. *Cell* **186**, 4117–4133 (2023).
26. Morin, J., Rolland, Y., Bischoff-Ferrari, H. A., Ocampo, A. & Perez, K. Association between prescription drugs and all-cause mortality risk in the UK population. *Aging Cell* <https://doi.org/10.1111/ace1.14334> (2024).
27. Faubion, S. S., Kuhle, C. L., Shuster, L. T. & Rocca, W. A. Long-term health consequences of premature or early menopause and considerations for management. *Climacteric* **18**, 483–491 (2015).
28. Frakes, A. E. et al. Four glial cells regulate ER stress resistance and longevity via neuropeptide signaling in *C. elegans*. *Science* **367**, 436–440 (2020).
29. Sheng, L. et al. Ensheathing glia promote increased lifespan and healthy brain aging. *Aging Cell* **22**, e13803 (2023).
30. Tokizane, K., Brace, C. S. & Imai, S. DMH^{Ppp1r17} neurons regulate aging and lifespan in mice through hypothalamic-adipose inter-tissue communication. *Cell Metab.* **36**, 377–392 (2024).
31. Koren, T. et al. Insular cortex neurons encode and retrieve specific immune responses. *Cell* **184**, 5902–5915 (2021).
32. Osterhout, J. A. et al. A preoptic neuronal population controls fever and appetite during sickness. *Nature* **606**, 937–944 (2022).
33. Poller, W. C. et al. Brain motor and fear circuits regulate leukocytes during acute stress. *Nature* **607**, 578–584 (2022).
34. Cathomas, F. et al. Circulating myeloid-derived MMP8 in stress susceptibility and depression. *Nature* **626**, 1108–1115 (2024).
35. Jin, H., Li, M., Jeong, E., Castro-Martinez, F. & Zuker, C. S. A body-brain circuit that regulates body inflammatory responses. *Nature* **630**, 695–703 (2024).
36. Wen, J. et al. The genetic architecture of biological age in nine human organ systems. *Nat. Aging* **4**, 1290–1307 (2024).
37. Foy, B. H. et al. Haematological setpoints are a stable and patient-specific deep phenotype. *Nature* **637**, 430–438 (2025).
38. Smith, S. M., Miller, K. L. & Nichols, T. E. Characterising ongoing brain aging and baseline effects from cross-sectional data. Preprint at *bioRxiv* <https://doi.org/10.1101/2025.01.21.634044> (2025).
39. Bonaccio, M. et al. Age-sex-specific ranges of platelet count and all-cause mortality: prospective findings from the MOLI-SANI study. *Blood* **127**, 1614–1616 (2016).
40. Aune, D. et al. BMI and all cause mortality: systematic review and non-linear dose-response meta-analysis of 230 cohort studies with 3.74 million deaths among 30.3 million participants. *BMJ* **353**, i2156 (2016).
41. Karaphillis, E., Goldstein, R., Murphy, S. & Qayyum, R. Serum alanine aminotransferase levels and all-cause mortality. *Eur. J. Gastroenterol. Hepatol.* **29**, 284–288 (2017).
42. Ikram, M. A. The use and misuse of 'biological aging' in health research. *Nat. Med.* **30**, 3045 (2024).
43. Ulrich-Lai, Y. M. & Herman, J. P. Neural regulation of endocrine and autonomic stress responses. *Nat. Rev. Neurosci.* **10**, 397–409 (2009).
44. Tracey, K. J. The inflammatory reflex. *Nature* **420**, 853–859 (2002).
45. Wang, F. et al. Myelin degeneration and diminished myelin renewal contribute to age-related deficits in memory. *Nat. Neurosci.* **23**, 481–486 (2020).
46. Depp, C. et al. Myelin dysfunction drives amyloid- β deposition in models of Alzheimer's disease. *Nature* **618**, 349–357 (2023).
47. Crapser, J. D., Arreola, M. A., Tsourmas, K. I. & Green, K. N. Microglia as hackers of the matrix: sculpting synapses and the extracellular space. *Cell. Mol. Immunol.* **18**, 2472–2488 (2021).
48. Crapser, J. D. et al. Microglia facilitate loss of perineuronal nets in the Alzheimer's disease brain. *eBioMedicine* **58**, 102919 (2020).
49. Nott, A. et al. Brain cell type-specific enhancer-promoter interactome maps and disease risk association. *Science* **366**, 1134–1139 (2019).

Publisher's note Springer Nature remains neutral with regard to jurisdictional claims in published maps and institutional affiliations.

Open Access This article is licensed under a Creative Commons Attribution-NonCommercial-NoDerivatives 4.0 International License, which permits any non-commercial use, sharing, distribution and reproduction in any medium or format, as long as you give appropriate credit to the original author(s) and the source, provide a link to the Creative Commons licence, and indicate if you modified the licensed material. You do not have permission under this licence to share adapted material derived from this article or parts of it. The images or other third party material in this article are included in the article's Creative Commons licence, unless indicated otherwise in a credit line to the material. If material is not included in the article's Creative Commons licence and your intended use is not permitted by statutory regulation or exceeds the permitted use, you will need to obtain permission directly from the copyright holder. To view a copy of this licence, visit <http://creativecommons.org/licenses/by-nc-nd/4.0/>.

© The Author(s) 2025

Methods

UKB

Participants and proteomics. The UKB is a population-based prospective cohort with omics and phenotypic data collected on approximately 500,000 participants, aged 40–69 years at recruitment, between 2006 and 2010. A subset of participants had subsequent visits after the baseline assessment: 20,337 participants had a first repeat assessment (Instance 1; 2012–2013); approximately 85,000 had a first MRI imaging visit (Instance 2; from 2014 to ongoing); and approximately 9,000 had a second MRI imaging visit (Instance 3; from 2019 to ongoing). Details on available phenotypes can be found at <https://biobank.ndph.ox.ac.uk/showcase/>, and all participants provided informed consent.

The UKB-PPP consortium generated Olink Explore 3,072 proteomics data from blood plasma samples collected from 54,219 UKB participants. These data consisted of 46,595 randomly selected samples from the baseline visit and 6,376 additional baseline visit samples selectively prioritized by the UK-PPP (samples presumably enriched for rare diseases and polymorphisms). Additional Olink proteomics data (using an earlier version of the platform, ~1,500 proteins) were generated from 1,268 participants who participated in the COVID-19 repeat imaging study. These data included samples from the baseline visit, Instance 2 (imaging visit 2014+) and Instance 3 (imaging visit 2019+). Additional details on the proteomics data are provided in Sun et al.¹⁰ and at https://biobank.ndph.ox.ac.uk/ukb/ukb/docs/PPP_Phase_1_QC_dataset_companion_doc.pdf.

UKB data were analyzed under application number 45420.

Clinical phenotypes. We defined participants' last known age as either age at death or the difference between the latest date available in International Classification of Diseases (ICD)-9, ICD-10, operating procedure, cancer registry or UKB assessment visit fields and birth date; this age corresponds to censoring in the following survival analyses. Additionally, we define the age at onset of several groups of diseases based on a combination of information in ICD-10, ICD-9, operating procedure and cancer registry. The following disease groups were defined, as in ref. 50: Type 2 diabetes (E11), Ischemic heart disease (I20 to I25), Cerebrovascular disease (I60 to I69), Chronic liver disease (K70 and K73 to K76), Chronic kidney disease (N18), All-cause dementia (A81, F00 to F03, F05, F10, G30, G31 and I67), Vascular dementia (F01 and I67), Alzheimer's disease (F00 and G30), Parkinson's disease and parkinsonism (G20 to G22), Rheumatoid arthritis (M05 and M06), Macular degeneration (H35), Osteoporosis (M80 and M81), Osteoarthritis (M15 to M19), Prevalent hypertension (I10 to I13 and I15), Colorectal cancer (C18 to C20), Lung cancer (C33 and C34), Esophageal cancer (C15), Liver cancer (C22), Pancreatic cancer (C25), Brain cancer (C71), Leukemia (C91 to C95), Non-Hodgkin lymphoma (C82 to C86), Breast cancer (C50), Ovarian cancer (C56 and C57) and Prostate cancer (C61). For heart-related diseases, the group definitions were based on ref. 51: Heart failure (ICD-9: 4254, 4280, 4281 and 4289; ICD-10: I110, I130, I132, I255, I420, I428, I429, I500, I501 and I509) and Atrial fibrillation or flutter (ICD-9: 4273; ICD-10: I480, I481, I482, I483, I484 and I489; OPCS-4: K571, K621, K622, K623, K624, X501 and X502).

The following lifestyle and socioeconomic factors were assessed: alcohol intake frequency, smoking status, number of days per week of moderate physical activity 10+ minutes, number of days per week of vigorous physical activity 10+ minutes, Townsend Deprivation Index, sleeplessness or insomnia, age at completed full-time education, oily fish intake, beef intake, cooked vegetable intake, tea intake, pork intake, processed meat intake, salad raw vegetable intake, bread intake, fresh fruit intake, non-oil fish intake and poultry intake. Medications reported in the verbal interview (<https://biobank.ctsu.ox.ac.uk/crystal/label.cgi?id=100075>) were also analyzed with a minimum of 100 participants per medication. Brain MRI-derived phenotypes extracted with FreeSurfer version 6 (<https://biobank.ctsu.ox.ac.uk/crystal/label.cgi?id=110> and <https://biobank.ctsu.ox.ac.uk/crystal/>

[refer.cgi?id=1977](https://biobank.ctsu.ox.ac.uk/crystal/label.cgi?id=1977)) were analyzed, and age at MRI as well as estimated total intracranial volume were regressed out.

Proteomics quality control and imputation. The post-UKB-PPP quality control baseline visit data consist of 2,923 protein measurements from 53,018 samples. We performed additional quality control steps (Supplementary Fig. 2a) in the following order: 8,182 samples with more than 1,000 protein missing values were removed; seven proteins with missing values in over 10% of samples were removed; and 338 samples with discordant reported sex and genetic sex were removed. This resulted in a post-quality control dataset consisting of 44,498 samples with 2,916 protein measurements.

We then performed missing value imputation of the proteomics data (Supplementary Fig. 2b) with the following steps. First, we split the data into train and test, with each split comprising 11 randomly selected centers (train centers: 11002, 11005, 11006, 11007, 11008, 11009, 11013, 11014, 11017, 11018 and 11023; test centers: 10003, 11001, 11003, 11004, 11010, 11011, 11012, 11016, 11020, 11021 and 11022). Protein values were z-score normalized based on the means and standard deviations of protein values in the train split. We trained a *k*-nearest neighbors imputer using scikit-learn's KNNImputer function with the number of neighbors (*k*) set to the square root of the sample size of the train split (*k* = 152). We evaluated the imputer on a subset of 5,591 samples (2,967 train and 2,624 test) with zero original missing values. Specifically, we randomly inserted missing values into this 'ground truth' subsample at a rate equivalent to the missing value rate in the whole post-quality control dataset (3%). We then performed imputation on this subsample to calculate the error between imputed values and original ground truth values. We confirmed robust imputation with a total MAE of 0.57 (Supplementary Fig. 2c,d), which was consistent across both train and test. This is a relatively small error, considering that the data distribution is approximately 5 (*z*-score ± 2.5 covers 99% of the distribution).

Stanford

Participants. *Stanford ADRC.* Samples were acquired through the National Institute on Aging-funded Stanford ADRC. The Stanford ADRC cohort is a longitudinal observational study of individuals with clinical dementia and age-matched and sex-matched individuals without dementia. All healthy control participants were deemed cognitively unimpaired during a clinical consensus conference that included board-certified neurologists and neuropsychologists. Cognitively impaired participants underwent Clinical Dementia Rating and standardized neurological and neuropsychological assessments to determine cognitive and diagnostic status, including procedures of the National Alzheimer's Coordinating Center (<https://naccdata.org/>). Cognitive status was determined in a clinical consensus conference that included neurologists and neuropsychologists. All participants were free from acute infectious diseases and in good physical condition.

SAMS. SAMS is an ongoing longitudinal study of healthy aging. Blood and cerebrospinal fluid (CSF) collection and processing were done by the same team and using the same protocol as in the Stanford ADRC. Neurological and neuropsychological assessments were performed by the same team and using the same protocols as in the Stanford ADRC. All SAMS participants had Clinical Dementia Rating = 0 and a neuropsychological test score within the normal range, and all SAMS participants were deemed cognitively unimpaired during a clinical consensus conference that included neurologists and neuropsychologists.

Sample preparation and proteomics. Plasma and CSF collection, processing and storage for all Stanford cohorts were performed using a single standard operating procedure. All studies were approved by the institutional review board of Stanford University, and written informed

consent or assent was obtained from all participants or their legally authorized representative.

Blood collection and processing were done according to a rigorous standardized protocol to minimize variation associated with blood draw and blood processing. In brief, approximately 10 cc of whole blood was collected in four vacutainer EDTA tubes (Becton Dickinson) and spun at 1,800g for 10 minutes to separate out plasma, leaving 1 cm of plasma above the buffy coat and taking care not to disturb the buffy coat to circumvent cell contamination. Plasma was aliquoted into polypropylene tubes and stored at -80°C . Plasma processing times averaged approximately 1 hour from the time of the blood draw to the time of freezing and storage. All blood draws were done in the morning to minimize the impact of circadian rhythm on protein concentrations. CSF was collected via lumbar puncture using a 20–22-gauge spinal needle that was inserted in the L4–L5 or L5–S1 interspace. CSF samples were immediately centrifuged at 500g for 10 minutes, aliquoted in polypropylene tubes and stored at -80°C .

Olink Explore 3,072 plasma proteomics data from 601 samples with matched SomaScan plasma proteomics data were analyzed in this study.

Computational Analyses

Identification of organ-enriched plasma proteins. We used the same methods that we developed in our previous study⁴ to identify putative plasma proteins. In brief, we identified organ-enriched genes: genes that were expressed at least four times higher in a single organ compared to any other organ based on human tissue bulk RNA sequencing data from the Gene Tissue Expression Atlas (Supplementary Fig. 1a–d). We refer to our previous study for details⁴. Our classification of organ-enriched genes is provided in Supplementary Table 1. We mapped these genes to proteins measured by Olink to identify organ-enriched plasma proteins in the UKB dataset (Supplementary Table 2). Non-organ-enriched plasma proteins were called ‘organismal’ proteins.

We compared our transcriptomics-based organ enrichment classification to proteomics-based organ enrichment from Jiang et al.⁵². Forty-eight of the 2,916 plasma proteins in the UKB dataset were not detected in Jiang et al. tissue proteomics data. Of the detected proteins, 80% of those we called ‘organ-enriched’ were also called organ-enriched or organ-specific in the same organ in Jiang et al. (Supplementary Fig. 1e), suggesting strong concordance between RNA and protein-based enrichment classification. Twelve percent of our organ-enriched plasma proteins were not enriched in Jiang et al., and 8% were enriched in a different organ (Supplementary Fig. 1e). Most of the discordant proteins (20%) were secreted proteins produced by the liver; we called these proteins ‘liver-enriched’ based on RNA, but, based on Jiang et al. tissue proteomics, they were called either artery-enriched or non-enriched (Supplementary Fig. 1f,g). This highlights a key distinction between organ enrichment classification based on tissue transcriptomics versus proteomics: transcriptomics captures the source of the protein, whereas proteomics captures its destination. Although understanding inter-organ communication by studying the source versus destination of proteins is an interesting area for future study, for our current study, our goal was to determine the putative organ source of plasma proteins to infer organ age.

Organ age estimation and age gap calculation. We used LASSO regression models to build chronological age predictors (also known as aging models) to estimate biological age. Aging models were trained and tested on the post-quality control imputed baseline visit proteomics data, using the same train–test split as the imputation. The LassoCV function from the scikit-learn⁵³ Python package was used to identify the optimal lambda parameter value using five-fold cross-validation. The lambda value that achieved 95% of the performance of the highest-performing lambda value was applied to scikit-learn’s LASSO function to derive sparse aging models. Each organ aging model was

trained using a distinct set of organ-enriched plasma proteins. An organismal aging model was trained using non-organ-enriched proteins. A conventional aging model was trained using all proteins. Age gaps were calculated as the residual of predicted age linearly regressed against actual age. Age gaps were z-scored per aging model to normalize for differences in age prediction accuracy. z-scored age gaps were used for all analyses. Extreme agers were defined as individuals with an age gap z-score greater than 1.5 or a z-score less than -1.5 in a given aging model. Conventional age gaps were not included in the extreme ager analyses due to their high similarity to organismal age gaps (Fig. 1b,c). All aging model weights are provided in Supplementary Table 3.

In addition to aging models trained on only proteins, we also assessed aging models trained on proteins and sex as well as aging models trained separately per sex. Pairwise correlations between age gaps produced by these different modeling frameworks showed very similar age gaps between the different modeling frameworks (Supplementary Fig. 3a). Age gap associations with mortality were highly similar across frameworks (Supplementary Fig. 3b). Extreme ager associations with mortality were similar, but sex-specific models showed no significant associations between extreme youth and longevity, although brain and immune youth trended toward significance (Supplementary Fig. 3c). For simplicity and robustness, we focused on aging models trained on only proteins for all primary analyses in this paper.

We also assessed aging models trained on only the randomly selected participants (86%) in the dataset. As mentioned previously, 14% of the samples were prioritized by the UKB-PPP to study specific diseases of interest. Aging models trained on the whole dataset and aging models trained on only the randomly selected subset produced nearly equivalent age gaps ($r = 1.00$; Supplementary Fig. 4a). Age gap associations with incident disease and mortality were also nearly equivalent when examining either all participants or only randomly selected participants ($r = 0.99$ and $r = 0.99$; Supplementary Fig. 4b,c). Given these consistencies, we analyze the entire dataset in this paper.

Longitudinal age gap analyses. Longitudinal age gap analyses (Extended Data Fig. 3) required use of plasma proteomics data collected across multiple visits (baseline, Instance 2 and Instance 3) from the same individual. However, proteomics data from post-baseline samples were obtained from an earlier version of the Olink assay with 1,459 proteins and were not compatible with models trained on the approximately 3,000-protein platform. Therefore, for longitudinal age gap analyses, we trained a distinct set of organ aging models using the subset of 1,459 proteins that were measured across all visits.

Four proteins with missing values in over 10% of samples were removed, leaving 1,459 proteins for model development. For model training, missing values for baseline samples were *k*-nearest neighbor imputed as described above. 1,500-protein-based aging models were trained on 44,406 baseline samples from individuals who did not have follow-up proteomics data. Samples from individuals with longitudinal proteomics data were not included in model training to prevent model training/evaluation contamination. 1,500-protein-based aging models were LASSO regression models trained to predict the predicted age from the 3,000-protein-based organ aging models. To maximize the number of testable samples with unimputed data, we aimed to maximize sparsity of the models. The lambda value that achieved 90% of the performance of the highest-performing lambda value was used, followed by recursive feature elimination using scikit-learn’s RFECV function. Liver and muscle 1,500-based aging models were removed due to low correlation ($r < 0.8$) with 3,000-based aging models.

Models were tested and evaluated on longitudinal data from 1,176 unique individuals who had non-missing values for all remaining aging model proteins (880 baseline, 843 Instance 2 and 786 Instance 3 samples). The mean number of years between Instance 2 and baseline was 9.1 years (s.d. = 1.8), and the mean number of years between Instance 3 and Instance 2 was 3.3 years (s.d. = 1.6).

MRI-based brain age estimation. We trained an MRI-based brain aging model using 479 FreeSurfer brain volumetric phenotypes from 45,574 individuals from Instance 2 (Extended Data Fig. 5d). This model was trained using the same pipeline as used for the organ aging models (LassoCV, five-fold cross-validation, lambda value with 95% performance). MRI brain age gaps from Instance 2 were correlated with plasma brain age gaps from baseline.

Statistical analyses. Cox proportional hazard regression (CoxPHFitter function from the lifelines⁵⁴ Python package) was used to assess the associations between organ age gaps and future disease or mortality risk. Linear regression (OLS function from the statsmodels⁵⁵ Python package) was used to assess the associations between organ age gaps and environmental factors recorded at the time of blood draw. All Cox and linear regression models included age and sex as additional covariates. Multiple hypothesis testing correction was applied, when appropriate, using the Benjamini–Hochberg method, and the significance threshold was a 5% false discovery rate. Corrected *P* values are referred to in this paper as *q* values. Gene Ontology pathway enrichment analyses were performed using gProfiler⁵⁶.

Reporting summary

Further information on research design is available in the Nature Portfolio Reporting Summary linked to this article.

Data availability

UK Biobank data are available upon request to qualified researchers through a standard protocol (<https://www.ukbiobank.ac.uk/register-apply>). Organ age estimates for all participants analyzed in this study will be made available to UK Biobank researchers through Showcase. Stanford Olink/SomaScan from plasma/CSF and associated patient metadata are available upon reasonable request to the Stanford ADRC data release committee (<https://web.stanford.edu/group/adrc/cgi-bin/web-proj/datareq.php>). Data from specific Stanford cohorts can be requested to the following cohort leaders: ADRC, T.W.-C. (twc@stanford.edu); SAMS, E.M. (bmormino@stanford.edu) or A.D.W. (awagner@stanford.edu). Raw tissue bulk RNA sequencing data from the Adult Genotype Tissue Expression (GTEx) Project are available at the GTEx website (<https://www.gtexportal.org/home/aboutAdultGtex>). Public brain single-cell RNA sequencing datasets used in this study²³ are available in the Gene Expression Omnibus under accession code GSE254205.

Code availability

Aging models are linear models with coefficients for specific proteins and an intercept value. Predicted age is the linear combination of protein coefficients and z-scored protein levels, plus the intercept value. All aging model coefficients are provided in Supplementary Table 3. A Python tutorial on applying these coefficients to independent datasets is available in the organageUKB GitHub repository (<https://github.com/hamiltonoh/organageUKB>).

References

- Argentieri, M. A. et al. Proteomic aging clock predicts mortality and risk of common age-related diseases in diverse populations. *Nat. Med.* **30**, 2450–2460 (2024).
- Schuermans, A. et al. Integrative proteomic analyses across common cardiac diseases yield mechanistic insights and enhanced prediction. *Nat. Cardiovasc. Res.* **3**, 516–1530 (2024).
- Jiang, L. et al. A quantitative proteome map of the human body. *Cell* **183**, 269–283 (2020).
- Pedregosa, F. et al. Scikit-learn: machine learning in Python. *J. Mach. Learn. Res.* **12**, 2825–2830 (2011).
- Davidson-Pilon, C. lifelines, survival analysis in Python (v0.27.0). *Zenodo* <https://doi.org/10.5281/zenodo.6359609> (2022).
- Seabold, S. & Perktold, J. Statsmodels: econometric and statistical modeling with Python. In *Proc. 9th Python in Science Conference* (eds van der Walt, S. & Millman, J.) 92–96 (2010).
- Raudvere, U. et al. g:Profiler: a web server for functional enrichment analysis and conversions of gene lists (2019 update). *Nucleic Acids Res.* **47**, W191–W198 (2019).

Acknowledgements

We thank B. Lehallier, A. Antebi, L. Gold and members of the Wyss-Coray laboratory for feedback and support and D. Channappa for laboratory management. This work was supported by the Stanford Alzheimer's Disease Research Center (National Institute on Aging grants P50AGO47366 and P30AGO66515); the National Institute on Aging (AGO72255, T.W.-C.); the Milky Way Research Foundation (T.W.-C.); and the Knight Initiative for Brain Resilience (T.W.-C.). The Stanford Aging and Memory Study was supported by the National Institutes of Health (NIH) (R01AGO48076, A.D.W.; R21AGO58859, E.C.M.), the Stanford Wu Tsai Neurosciences Institute (E.C.M. and A.D.W.) and the Stanford Center for Precision Health and Integrated Diagnostics (PHIND) (A.D.W. and E.C.M.). This work was further supported by the Stanford Graduate Fellowship (H.S.O.), the National Science Foundation Graduate Research Fellowship (H.S.O.) and the NIH Center for Clinical and Translational Education and Research award, Biostatistics, Epidemiology and Research Design (BERD) program (UL1TR003142, Y.L.G.).

Author contributions

H.S.-H.O., J.R. and T.W.-C. conceptualized the study. H.S.-H.O. led study design and analyses. Y.L.G. led data processing of UK Biobank clinical phenotypes and advised on analyses. N.R. aided in longitudinal organ age gap analyses and figure generation. D.Y.U. aided in disease progression analyses and figure generation. A.F. aided in Stanford data generation and analyses. A.D.W. and E.M. led the SAMS cohort. A.D.W., A.B., J.R. and M.D.G. provided key insights. H.S.-H.O. produced figures and wrote the paper. T.W.-C. edited the paper. T.W.-C. supervised the study. All authors critically revised the paper for intellectual content. All authors read and approved the final version of the paper.

Competing interests

T.W.-C., H.S.-H.O. and J.R. are co-founders and scientific advisors of Teal Omics, Inc. and have received equity stakes. T.W.-C. is co-founder of Vero Biosciences. The remaining authors declare no competing interests.

Additional information

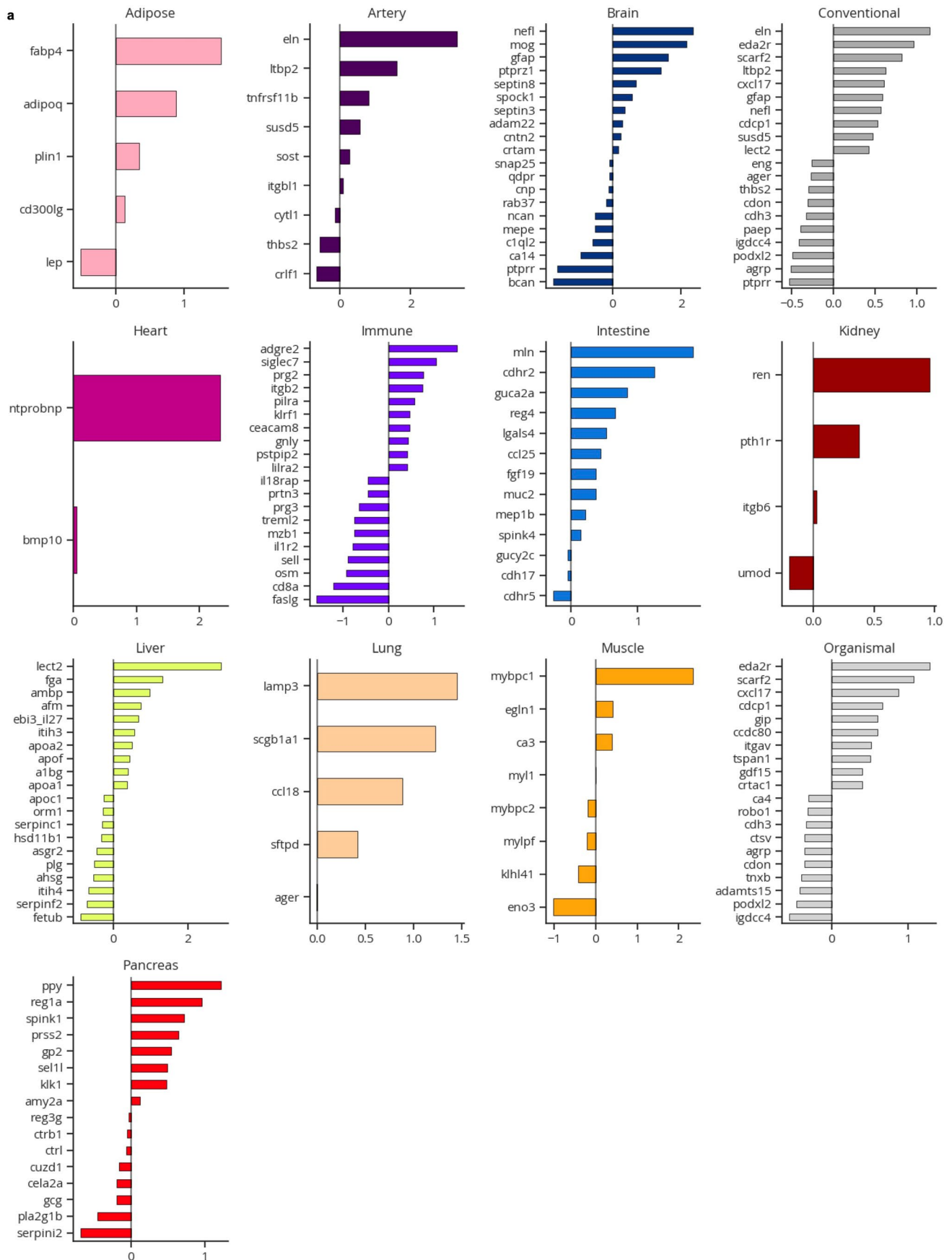
Extended data is available for this paper at <https://doi.org/10.1038/s41591-025-03798-1>.

Supplementary information The online version contains supplementary material available at <https://doi.org/10.1038/s41591-025-03798-1>.

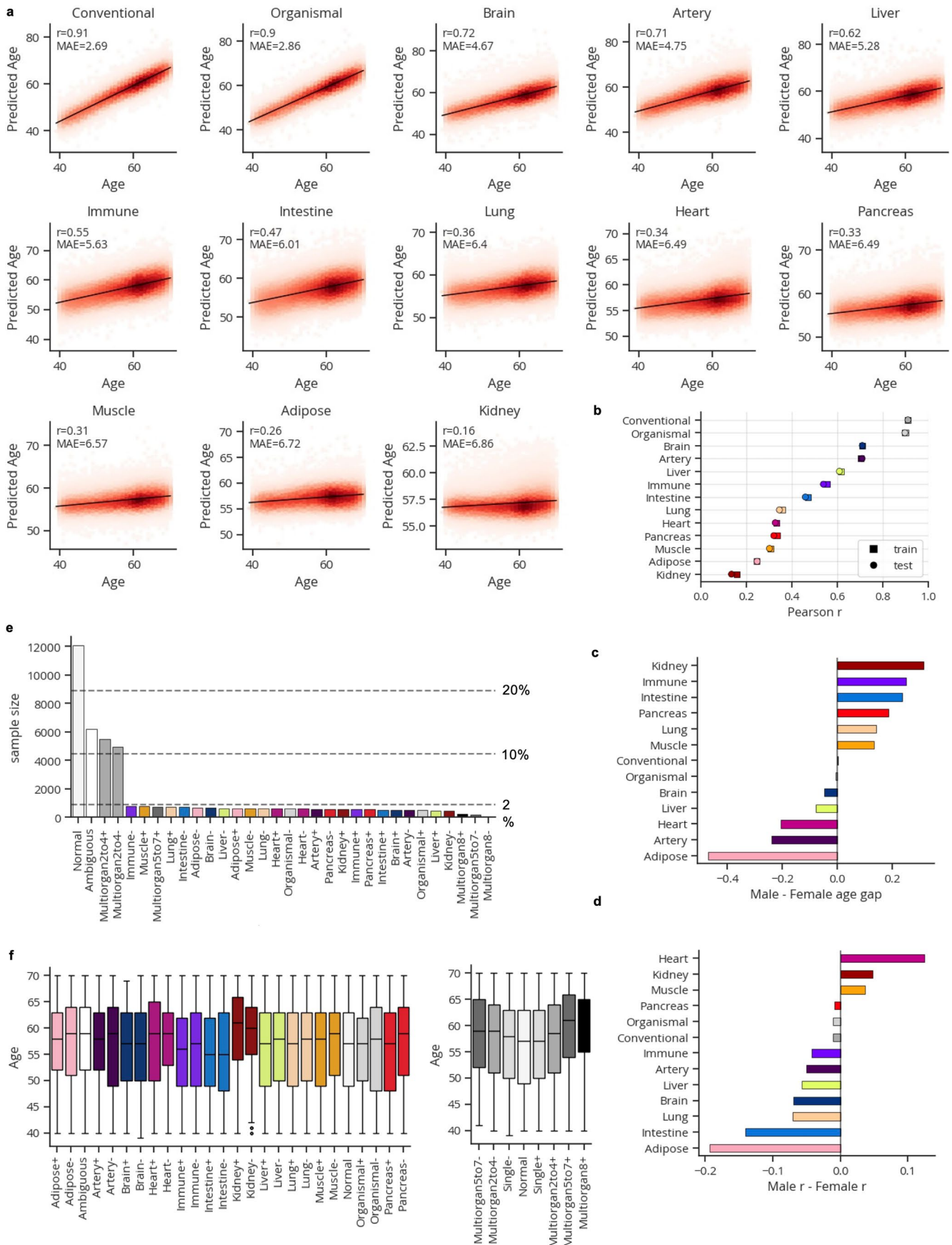
Correspondence and requests for materials should be addressed to Hamilton Se-Hwee Oh or Tony Wyss-Coray.

Peer review information *Nature Medicine* thanks Bradford Gibson and the other, anonymous, reviewer(s) for their contribution to the peer review of this work. Primary Handling Editor: Michael Basson, in collaboration with the *Nature Medicine* team.

Reprints and permissions information is available at www.nature.com/reprints.



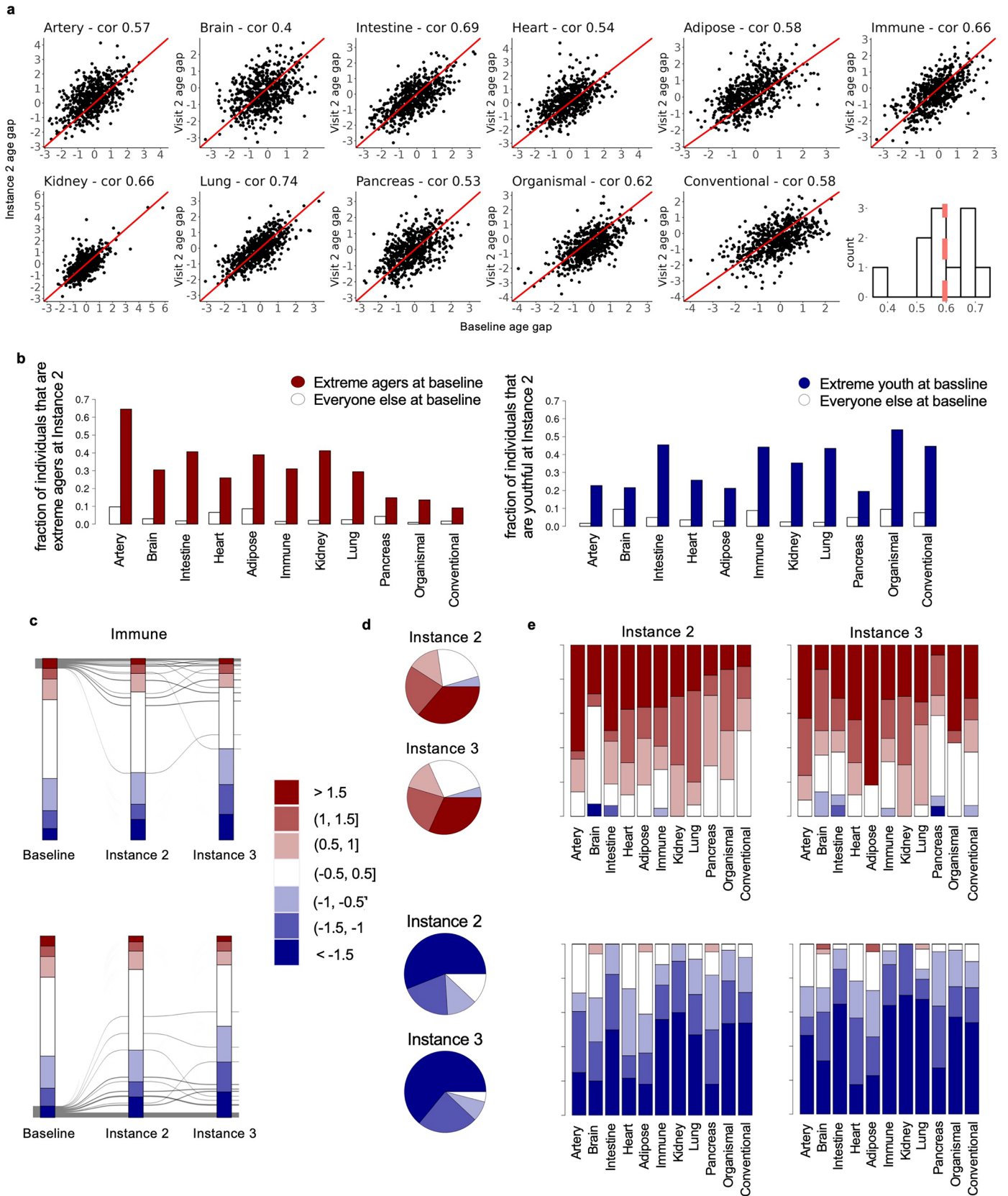
Extended Data Fig. 1 | Aging model coefficients. a. For all aging models, the top 20 aging model proteins and their weights are shown.



Extended Data Fig. 2 | See next page for caption.

Extended Data Fig. 2 | Organ aging models in the UK Biobank. **a**, Predicted organ age versus chronological age. Pearson correlations (r) and mean absolute errors (MAE) shown. **b**, Correlation between predicted and actual age across all aging models and train/test splits. **c**, Difference in correlation between predicted and actual age by biological sex. **d**, Mean difference in organ age gaps

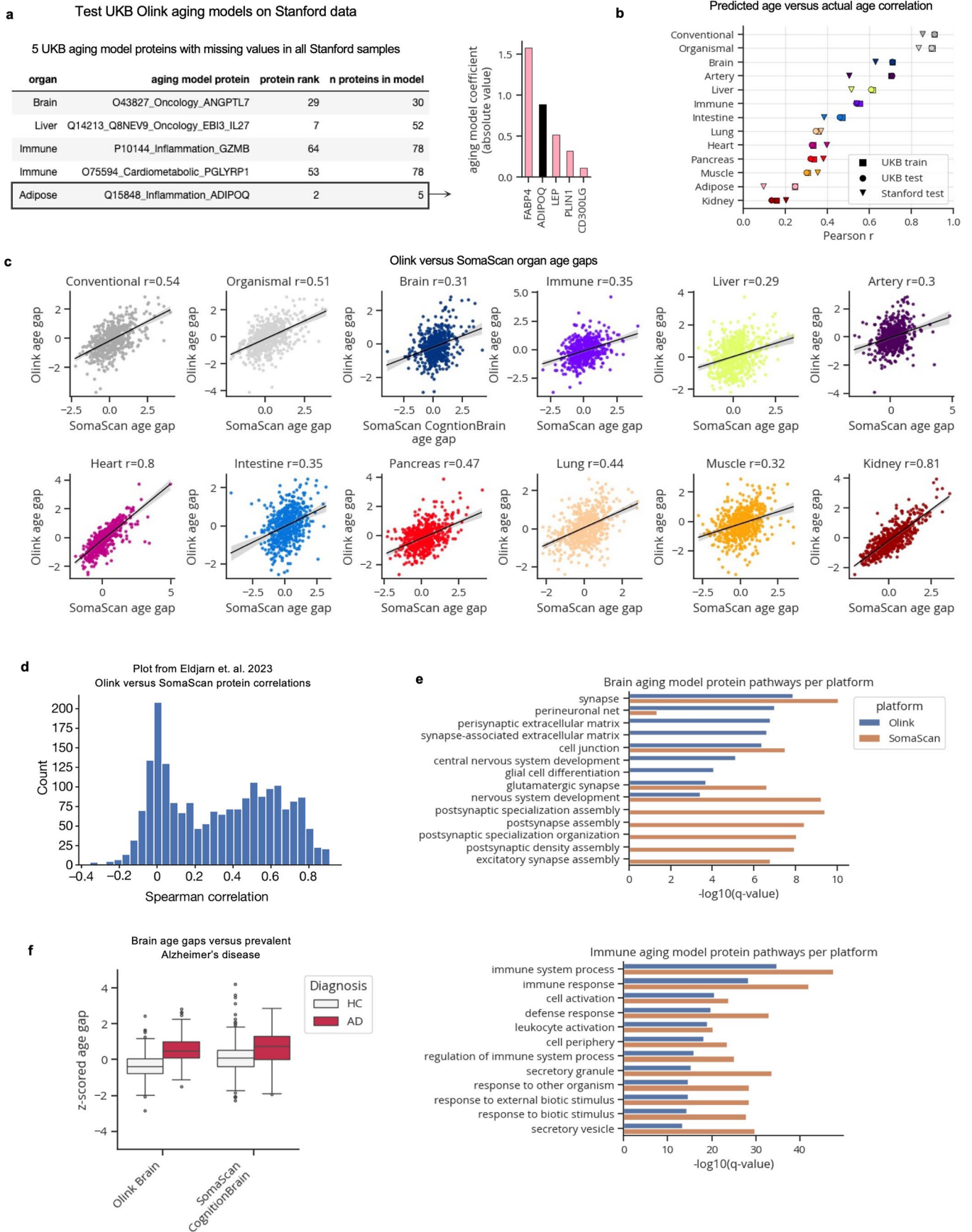
between males and females. **e**, Extreme ager sample sizes and proportions. **f**, Age distributions per extreme ager group ($n = 44,498$). The box bounds are the Q1, median and Q3; the whiskers show $Q1 - 1.5 \times$ the interquartile range (IQR) and $Q3 + 1.5 \times$ the IQR.



Extended Data Fig. 3 | See next page for caption.

Extended Data Fig. 3 | Age gaps across longitudinal visits. **a**, Longitudinal proteomics data from a subset of 1,176 individuals were analyzed (880 baseline, 843 Instance 2, and 786 Instance 3 samples). Longitudinal data were available only on the 1.5k-protein Olink assay, so new aging models trained on the 1.5k-assay were developed. New aging models were trained on 44,406 samples without longitudinal data and tested on non-imputed samples with longitudinal data. Only 1.5k-aging models with age estimates that were correlated $r > 0.8$ with 3k-based age estimates were included for downstream analyses. Correlation between baseline and Instance 2 age gaps are shown. **b**, Bar plot showing fractions of baseline extreme agers and non-extreme agers that are extreme

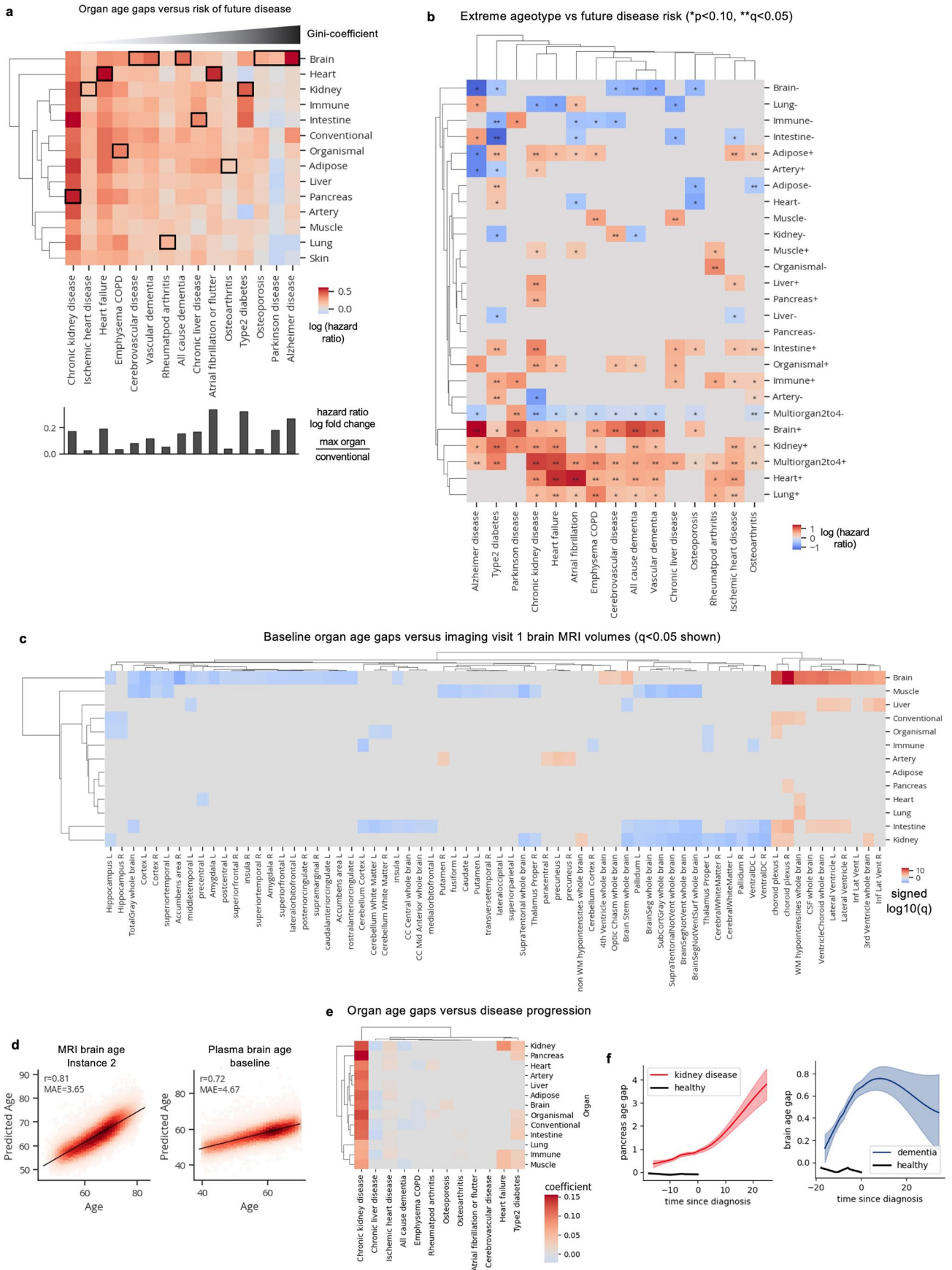
agers in the same organ in Instance 2. Equivalent plot for youthful agers is shown on the right. **c**, Age gaps were grouped into bins of 0.5 standard deviation to determine changes in age gap bins across visits. Individual trajectories across visits for extreme immune agers are shown. Equivalent plot for youthful immune agers is shown at the bottom. **d**, Pie chart showing percent distribution of immune age gap bins in Instance 2 and Instance 3 for individuals who are extreme immune agers at baseline. Equivalent plot for youthful immune agers is shown at the bottom. **e**, Stacked bar plot showing percent distribution of age gap bins in Instance 2 and Instance 3 for individuals who are extreme agers at baseline. Equivalent plot for youthful agers is shown at the bottom.



Extended Data Fig. 4 | See next page for caption.

Extended Data Fig. 4 | Olink versus SomaScan organ aging models. **a**, Stanford Olink data contained missing values for the 5 aging model proteins shown. Protein ranks by aging model coefficient compared to total number of proteins in aging model are shown. **b**, Correlation between predicted versus chronological age in UKB train, UKB test, and Stanford test (cognitively normal controls) data. **c**, Olink versus SomaScan (Oh and Rutledge et. al. 2023) organ age gaps in Stanford data. Linear regressions with 95% confidence intervals are shown.

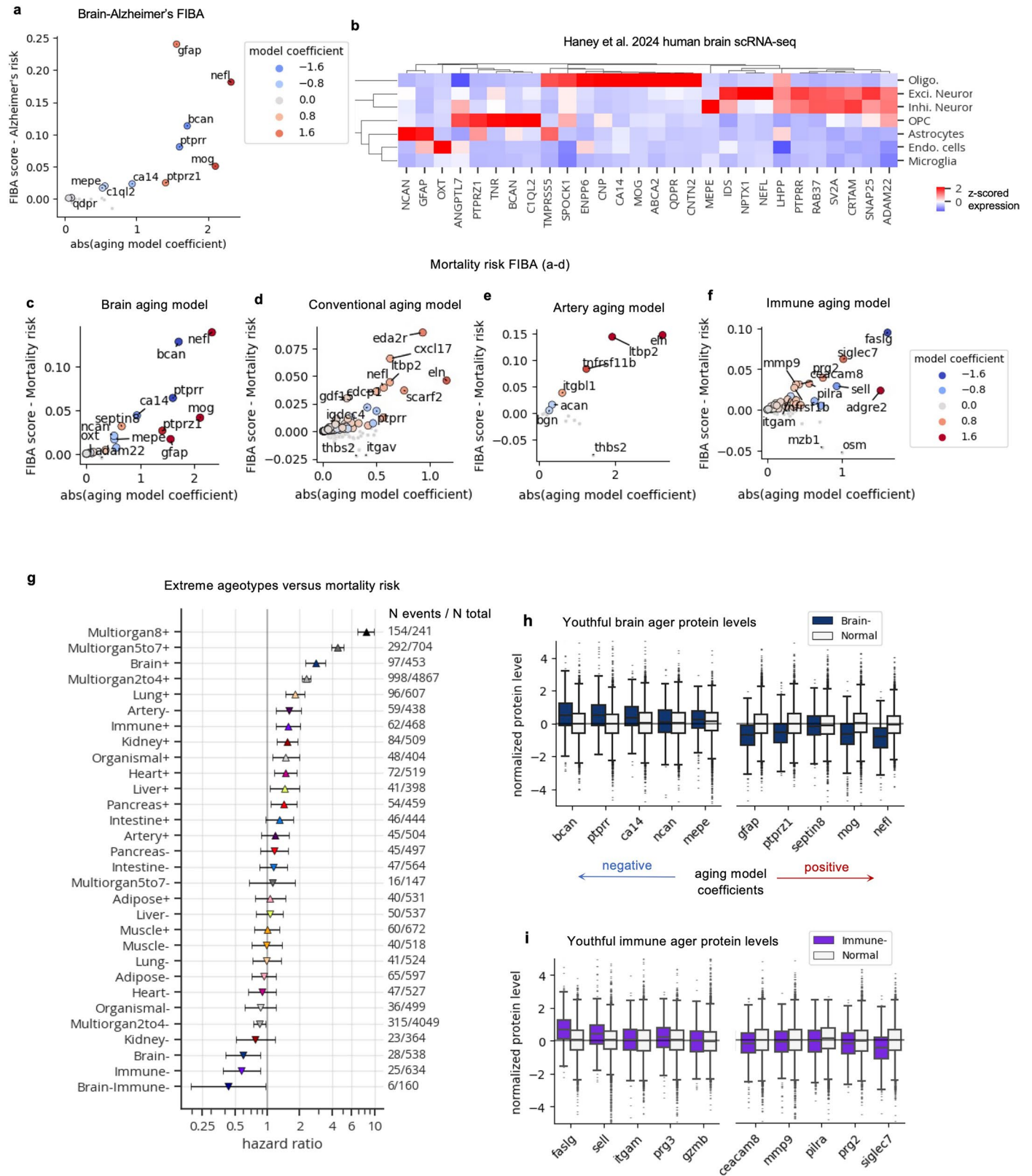
d, Distribution of correlations between Olink and SomaScan overlapping proteins by name (from Eldjarn et. al. 2023). **e**, g:Profiler biological pathway enrichment of brain and immune aging model proteins per proteomics platform. **f**, Brain age gaps versus Alzheimer's disease diagnosis, per proteomics platform (n = 598). The box bounds are the Q1, median and Q3; the whiskers show $Q1 - 1.5 \times$ the interquartile range (IQR) and $Q3 + 1.5 \times$ the IQR.



Extended Data Fig. 5 | See next page for caption.

Extended Data Fig. 5 | Age gaps versus disease. **a**, Cox proportional hazards regression was used to test the association between age gaps and future disease risk, adjusted for age-at-blood-draw and sex. Heatmap colored by age gap $\log(\text{hazard ratio})$ is shown. Heatmap columns are ordered by the Gini-coefficient of age gaps per disease. The most significant associations per disease are highlighted with black borders. The log fold change in hazard ratios between the organ with the most significant age gap versus the conventional age gap is shown below the heatmap. **b**, Cox proportional hazards regression was used to determine the association between extreme agers and future disease risk, controlling for age and sex and other extreme agers. Heatmap colored by age gap $\log(\text{hazard ratio})$ is shown. * $p < 0.05$, ** q (Benjamini-Hochberg correction) < 0.05 . Non-significant hazard ratios ($p < 0.05$) were set to zero. **c**, Linear regression was used to determine the association between baseline organ age

gaps and Instance 2 brain MRI volumes, controlling for age-at-blood-draw, age-at-MRI, sex, and estimated total intracranial volume. Non-significant effect sizes ($q < 0.05$) were set to zero. Red indicates positive associations, while blue indicates negative associations. **d**, MRI-based brain age versus chronological age in 45,574 individuals from Instance 2 (left). Plasma proteomics-based brain age versus chronological age in 44,498 individuals from baseline (right). Pearson correlations and mean absolute errors are shown. **e**, Linear regression was used to determine the association between organ age gaps and years since disease diagnosis. Non-significant effects ($q < 0.05$) were set to zero. **f**, Visualization of results from **e**. Organ age gap versus years since diagnosis shown for chronic kidney disease x pancreas age gap and Alzheimer's disease x brain age gap. Lowess regressions with 95% confidence intervals are shown.



Extended Data Fig. 6 | See next page for caption.

Extended Data Fig. 6 | Feature importance for organ aging, Alzheimer's disease, and mortality. a, Scatterplot showing results from feature importance for biological aging (FIBA) algorithm to identify proteins in the brain aging model contributing to the brain age gap's association with Alzheimer's disease risk. FIBA score (y-axis) indicates Alzheimer's disease risk effect size loss after permutation of protein values. X-axis indicates absolute protein weight in the brain aging model. Color indicates protein weight in the brain aging model. **b**, Mean gene expression of brain aging protein-encoding genes in Haney et al. 2024 human brain scRNA-seq data. **c-f**, Scatterplots showing results from feature importance for biological aging (FIBA) algorithm to identify proteins in the brain (c), conventional (d), artery (e), and immune (f) aging models that contribute to the model age gap's association with future mortality risk. FIBA score (y-axis) indicates mortality risk effect size loss after permutation of protein values. X-axis

indicates absolute protein weight in the aging model. Color indicates protein weight in the aging model. **g**, Forest plot showing results from Cox proportional hazards regression, testing the associations between extreme age status and future all-cause mortality risk, controlling for age, sex. Points show extreme age hazard ratios, error bars show 95% confidence intervals, and number on the right show number of events out of the total sample size. **h**, Protein levels of youthful brain agers versus normal agers (n = 12,696). The top ten (5 decrease with age, 5 increase with age) proteins based on mortality risk FIBA score are shown. Each protein was linearly adjusted for age, sex, and every other protein in the brain aging model before plotting. Proteins are ordered by the aging model coefficient. The box bounds are the Q1, median and Q3; the whiskers show Q1 - 1.5× the interquartile range (IQR) and Q3 + 1.5× the IQR. **i**, As in **h**, but for the immune aging model (n = 12,847).

Reporting Summary

Nature Portfolio wishes to improve the reproducibility of the work that we publish. This form provides structure for consistency and transparency in reporting. For further information on Nature Portfolio policies, see our [Editorial Policies](#) and the [Editorial Policy Checklist](#).

Statistics

For all statistical analyses, confirm that the following items are present in the figure legend, table legend, main text, or Methods section.

n/a | Confirmed

- The exact sample size (n) for each experimental group/condition, given as a discrete number and unit of measurement
- A statement on whether measurements were taken from distinct samples or whether the same sample was measured repeatedly
- The statistical test(s) used AND whether they are one- or two-sided
Only common tests should be described solely by name; describe more complex techniques in the Methods section.
- A description of all covariates tested
- A description of any assumptions or corrections, such as tests of normality and adjustment for multiple comparisons
- A full description of the statistical parameters including central tendency (e.g. means) or other basic estimates (e.g. regression coefficient) AND variation (e.g. standard deviation) or associated estimates of uncertainty (e.g. confidence intervals)
- For null hypothesis testing, the test statistic (e.g. F , t , r) with confidence intervals, effect sizes, degrees of freedom and P value noted
Give P values as exact values whenever suitable.
- For Bayesian analysis, information on the choice of priors and Markov chain Monte Carlo settings
- For hierarchical and complex designs, identification of the appropriate level for tests and full reporting of outcomes
- Estimates of effect sizes (e.g. Cohen's d , Pearson's r), indicating how they were calculated

Our web collection on [statistics for biologists](#) contains articles on many of the points above.

Software and code

Policy information about [availability of computer code](#)

Data collection

Data analysis

```
Python 3.9.12
gprofiler-official==1.0.0
lifelines==0.27.3
matplotlib==3.5.1
numpy==1.21.5
pandas==1.4.2
scanpy==1.9.1
scikit-learn==1.0.2
scikit-survival==0.17.2
scipy==1.10.0
seaborn==0.12.2
statsmodels==0.13.5
```

```
R 4.1.2
metafor==4.2.0
```

Pre-calculated FreeSurfer v6 brain MRI volumes (<https://biobank.ctsu.ox.ac.uk/crystal/refer.cgi?id=1977>)

For manuscripts utilizing custom algorithms or software that are central to the research but not yet described in published literature, software must be made available to editors and reviewers. We strongly encourage code deposition in a community repository (e.g. GitHub). See the Nature Portfolio [guidelines for submitting code & software](#) for further information.

Data

Policy information about [availability of data](#)

All manuscripts must include a [data availability statement](#). This statement should provide the following information, where applicable:

- Accession codes, unique identifiers, or web links for publicly available datasets
- A description of any restrictions on data availability
- For clinical datasets or third party data, please ensure that the statement adheres to our [policy](#)

UK Biobank data is available upon request to qualified researchers through a standard protocol (<https://www.ukbiobank.ac.uk/register-apply>). Organ age estimates for all participants analyzed in this study will be made available to UK Biobank researchers through Showcase. Stanford Olink/SomaScan from plasma/CSF and associated patient metadata are available upon request to the to the Stanford-ADRC data release committee, <https://web.stanford.edu/group/adrc/cgi-bin/web-proj/datareq.php>. Data from specific Stanford cohorts can be requested to the following cohort leaders: ADRC, Tony Wyss-Coray (twc@stanford.edu); SAMS, Beth Mormino (bmormino@stanford.edu) or Anthony Wagner (awagner@stanford.edu). Raw tissue bulk RNA-seq data from the Adult Genotype Tissue Expression (GTEx) Project is available here (<https://www.gtexportal.org/home/aboutAdultGtex>). Public brain single-cell RNA-sequencing datasets used in this study¹ are available in the Gene Expression Omnibus under accession code GSE254205.

Research involving human participants, their data, or biological material

Policy information about studies with [human participants or human data](#). See also policy information about [sex, gender \(identity/presentation\), and sexual orientation](#) and [race, ethnicity and racism](#).

Reporting on sex and gender

Biological sex data was accessed through the UK Biobank portal. Only samples with concordant self reported and genetic sex were included. Organ age differences by sex were examined. Sex was used as a covariate in all disease-association regression models. Inclusion of sex in the organ aging models was assessed.

Reporting on race, ethnicity, or other socially relevant groupings

Data from all ethnicities in the UK Biobank plasma proteomics dataset was assessed.

Population characteristics

The UK Biobank is a volunteer based study. Plasma proteomics was performed on individuals aged 40-70 with equal distribution per sex.

UK Biobank

Participants and proteomics

The UK Biobank is a population-based prospective cohort with 'omics and phenotypic data collected on approximately 500,000 participants, aged 40 to 69 years at recruitment between 2006 and 2010. A subset participants had subsequent visits after the baseline assessment: 20,337 participants had a first repeat assessment (Instance 1; 2012-2013), approximately 85,000 had a first MRI imaging visit (Instance 2; from 2014 to ongoing), and approximately 9,000 had a second MRI imaging visit (Instance 3; from 2019 to ongoing). Details on available phenotypes can be found online at <https://biobank.ndph.ox.ac.uk/showcase/> and all participants provided informed consent.

The UK Biobank Pharma Proteomics Project (UKB-PPP) consortium generated Olink Explore 3,072 proteomics data from blood plasma samples collected from 54,219 UKB participants. These data consisted of 46,595 randomly selected samples from the baseline visit and 6,376 additional baseline visit samples selectively prioritized by the UK-PPP (samples presumably enriched for rare diseases and polymorphisms). Additional Olink proteomics data (using an earlier version of the platform, ~1,500 proteins) were generated from 1,268 participants who participated in the COVID-19 repeat imaging study. These data included samples from the baseline visit, Instance 2 (imaging visit 2014+) and Instance 3 (imaging visit 2019+). Further details on the proteomics data are described in Sun et al., 2023⁹ and https://biobank.ndph.ox.ac.uk/ukb/ukb/docs/PPP_Phase_1_QC_dataset_companion_doc.pdf.

Stanford

Participants

Stanford- Alzheimer's Disease Research Center (ADRC)

Samples were acquired through the National Institute on Aging (NIA)-funded Stanford Alzheimer's Disease Research Center (Stanford-ADRC). The Stanford-ADRC cohort is a longitudinal observational study of clinical dementia subjects and age-sex-matched nondemented subjects. All healthy control participants were deemed cognitively unimpaired during a clinical consensus conference that included board-certified neurologists and neuropsychologists. Cognitively impaired subjects underwent Clinical Dementia Rating and standardized neurological and neuropsychological assessments to determine cognitive and diagnostic status, including procedures of the National Alzheimer's Coordinating Center (<https://naccdata.org/>). Cognitive status was determined in a clinical consensus conference that included neurologists and neuropsychologists. All participants were free from acute infectious diseases and in good physical condition.

Stanford Aging and Memory Study (SAMS)

SAMS is an ongoing longitudinal study of healthy aging. Blood and CSF collection and processing were done by the same team and using the same protocol as in Stanford-ADRC. Neurological and neuropsychological assessments were performed by the same team and using the same protocol as in Stanford-ADRC. All SAMS participants had CDR=0 and a neuropsychological test score within the normal range; all SAMS participants were deemed cognitively unimpaired during a clinical consensus conference that included neurologists and neuropsychologists.

Sample preparation and proteomics

Plasma and CSF collection, processing, and storage for all Stanford cohorts were performed using a single standard operating procedure. All studies were approved by the Institutional Review Board of Stanford University and written informed consent or assent was obtained from all participants or their legally authorized representative.

Blood collection and processing were done according to a rigorous standardized protocol to minimize variation associated with blood draw and blood processing. Briefly, about 10cc of whole blood was collected in 4 vacutainer ethylenediaminetetraacetic acid (EDTA) tubes (Becton Dickinson vacutainer EDTA tube) and spun at 1800 x g for 10mins to separate out plasma, leaving 1cm of plasma above the buffy coat and taking care not to disturb the buffy coat to circumvent cell contamination. Plasma was aliquoted into polypropylene tubes and stored at -80oC. Plasma processing times averaged approximately one hour from the time of the blood draw to the time of freezing and storage. All blood draws were done in the morning to minimize the impact of circadian rhythm on protein concentrations. CSF was collected via lumbar puncture using a 20-22 G spinal needle that was inserted in the L4-L5 or L5-S1 interspace. CSF samples were immediately centrifuged at 500 x g for 10 mins, aliquoted in polypropylene tubes and stored at -80oC.

Olink Explore 3,072 plasma proteomics data from 601 samples with matched SomaScan plasma proteomics data were analyzed in this study. Ages ranged from 36-90 (mean=70, standard deviation=8).

Recruitment

The UK Biobank and Stanford are volunteer based, which may affect results, as they are not a true representative sample. 86% of the blood samples selected for proteomics were randomly selected. 14% were selected by the UKB-PPP.

Ethics oversight

The UK Biobank Ethics Advisory Committee. All Stanford studies were approved by the Institutional Review Board of Stanford University and written informed consent or assent was obtained from all participants or their legally authorized representative.

Note that full information on the approval of the study protocol must also be provided in the manuscript.

Field-specific reporting

Please select the one below that is the best fit for your research. If you are not sure, read the appropriate sections before making your selection.

Life sciences Behavioural & social sciences Ecological, evolutionary & environmental sciences

For a reference copy of the document with all sections, see nature.com/documents/nr-reporting-summary-flat.pdf

Life sciences study design

All studies must disclose on these points even when the disclosure is negative.

Sample size

All samples with plasma proteomics data were assessed.

Data exclusions

samples and proteins with limited missing values were analyzed. samples with concordant self-reported sex and genetic sex were included. details in the methods.

Replication

To ensure reproducibility and confidence in the findings, organ aging models were trained on ~half of the UK Biobank samples and tested on the other half. Performance was highly similar across train and test. Aging models were also tested on Stanford data, a completely independent dataset, and showed similar correlations between predicted and actual age. Mortality associations were also highly similar across train and test splits. All attempts at replication were successful.

Randomization

NA, no treatment group

Reporting for specific materials, systems and methods

We require information from authors about some types of materials, experimental systems and methods used in many studies. Here, indicate whether each material, system or method listed is relevant to your study. If you are not sure if a list item applies to your research, read the appropriate section before selecting a response.

Materials & experimental systems

- | | |
|-------------------------------------|--|
| n/a | Involved in the study |
| <input checked="" type="checkbox"/> | <input type="checkbox"/> Antibodies |
| <input checked="" type="checkbox"/> | <input type="checkbox"/> Eukaryotic cell lines |
| <input checked="" type="checkbox"/> | <input type="checkbox"/> Palaeontology and archaeology |
| <input checked="" type="checkbox"/> | <input type="checkbox"/> Animals and other organisms |
| <input checked="" type="checkbox"/> | <input type="checkbox"/> Clinical data |
| <input checked="" type="checkbox"/> | <input type="checkbox"/> Dual use research of concern |
| <input checked="" type="checkbox"/> | <input type="checkbox"/> Plants |

Methods

- | | |
|-------------------------------------|---|
| n/a | Involved in the study |
| <input checked="" type="checkbox"/> | <input type="checkbox"/> ChIP-seq |
| <input checked="" type="checkbox"/> | <input type="checkbox"/> Flow cytometry |
| <input checked="" type="checkbox"/> | <input type="checkbox"/> MRI-based neuroimaging |

Plants

Seed stocks

Report on the source of all seed stocks or other plant material used. If applicable, state the seed stock centre and catalogue number. If plant specimens were collected from the field, describe the collection location, date and sampling procedures.

Novel plant genotypes

Describe the methods by which all novel plant genotypes were produced. This includes those generated by transgenic approaches, gene editing, chemical/radiation-based mutagenesis and hybridization. For transgenic lines, describe the transformation method, the number of independent lines analyzed and the generation upon which experiments were performed. For gene-edited lines, describe the editor used, the endogenous sequence targeted for editing, the targeting guide RNA sequence (if applicable) and how the editor was applied.

Authentication

Describe any authentication procedures for each seed stock used or novel genotype generated. Describe any experiments used to assess the effect of a mutation and, where applicable, how potential secondary effects (e.g. second site T-DNA insertions, mosaicism, off-target gene editing) were examined.